

Research Paper

Three-dimensional discontinuous deformation analysis based on strain-rotation decomposition

Huo Fan^{a,*}, Hong Zheng^b, Jidong Zhao^{a,*}^a Department of Civil and Environmental Engineering, The Hong Kong University of Science and Technology, Clear Water Bay, Kowloon, Hong Kong^b State Key Laboratory of Geomechanics and Geotechnical Engineering, Chinese Academy of Sciences, Wuhan 430071, China

ARTICLE INFO

Keywords:

Three-dimensional dynamic deformation
 Discontinuous deformation analysis
 Strain-rotation decomposition
 Nonlinear analysis
 Nonphysical volume change

ABSTRACT

The strain and local rotation at any material point in a deformable body can be described by the strain-rotation (S-R) decomposition theorem. This paper presents a three-dimensional dynamic deformation formulation based on the S-R decomposition. The three-dimensional dynamic analysis formulation is generic and can be easily implemented into numerical methods. By combining the new formulation with the discontinuous deformation analysis (DDA), a new method named SR-3D-DDA is developed. We further use several examples to demonstrate that the S-R based DDA can help effectively eliminate the nonphysical volume change exhibited by existing DDAs and improve the accuracy of the predictions.

1. Introduction

Modern engineering design requires numerical tools to be developed in three-dimensional (3D) to be truly predictive. 3D formulations have therefore been implemented in mainstream numerical methods (see e.g. [1–19]). Frequently, numerical predictions of a practical 3D problem need to address challenges pertaining to various nonlinear behaviors, including material nonlinearity, contact nonlinearity and geometric nonlinearity. The conventional popular approaches include the total Lagrangian formulation (T.L.) and the updated Lagrangian formulation (U.L.) are all based on the Green's strain and polar decomposition theorem [20]. Recently, a new dynamic analysis formulation, based on strain-rotation (SR) decomposition theorem, has been proposed [21] to tackle geometric nonlinearity. It has demonstrated an advantage in simultaneously capturing the strain and local rotation reasonably well. However, it is only limited to two-dimensional cases. Meanwhile, as an alternative to describe the dynamic behavior of discontinuous media such as rock that involving discrete block system, 2D discontinuous deformation analysis (2D-DDA) [22] has been developed and has been extended to 3D as well [23]. DDA is able to conveniently simulate the translation, rotation and contact of blocks, while the fundamental unknowns can be made independent of the shapes of blocks. Various techniques have been developed to address the nonlinear behaviors, in particular the contact nonlinearity, based on new contact models [24] and contact resolution or detection algorithms [25–30]. A nodal-based 3D-DDA [31] and a particle-based 3D-DDA were further proposed [32] to enhance the predictive

capability of DDA to deal with the deformation of blocks. The bonding and cracking algorithm aiming at 3D particles were implemented [33]. The some latest advances in DDA can be found in [34]. However, there have been relatively scarce studies addressing the geometric nonlinearity in DDA.

An apparent pitfall in both 2D [35] and 3D [36] DDA methods is the false volume expansion predictions due to the adoption of first-order rotation approximation. A variety of mitigation methods have been proposed in the past for DDA, including the displacement adjustment method [35], the Taylor series method [37], the trigonometric method [38], and the displacement-strain modification method [39]. Amongst them, the 3D displacement adjustment method [36] appears to perform more robustly in suppressing the unreasonable volume expansion in 3D-DDA. However, in cases of “dual-axial rotation” and “tri-axial rotation” (to be defined in Section 4), the predictions by 3D displacement adjustment method may potentially result in nonphysical expansions in the direction(s) perpendicular to the rotation axis and nonphysical contractions in the direction parallel to the same rotation axis. So the geometrical shape of discrete block is forced to change non-physically though the volume of the block remains the same. The abovementioned expansion and contraction associated with 3D displacement adjustment method seems to have never been mentioned in the literature.

This study presents a substantial extension of the 2D dynamic deformation formulation previously proposed by the authors [21] to three-dimensional case. To effectively address the issue of geometric nonlinearity, a new formulation based on the S-R (strain-rotation) decomposition theorem [40–44] is developed which is generic and readily

* Corresponding authors.

E-mail addresses: huofan_hkust@163.com (H. Fan), jzhao@ust.hk (J. Zhao).

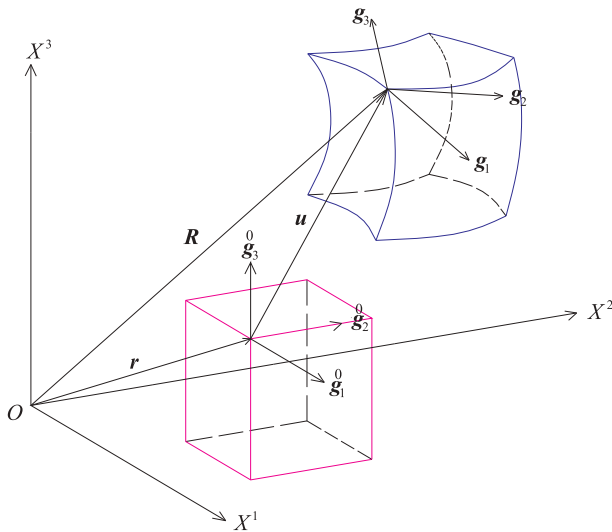


Fig. 1. A deformable body in three-dimension Euclidean space.

applicable to numerical method. The new S-R formulation is then implemented into 3D-DDA to form a new method termed SR-3D-DDA. Several examples are further presented to demonstrate that the advantage of the SR-3D-DDA in capturing the geometric nonlinearity of blocks. The study can offer an effective method in tackling a wide range of engineering problems involving discontinuous materials.

2. Three-dimensional dynamic formulation based on S-R decomposition

Considering the following deformable body in an Euclidean space in Fig. 1, where r and R are the position vectors of a point before and after deformation, respectively; and u is the displacement vector; g_i^0 and g_i ($i = 1, 2, 3$) represent two local basic vectors at a point corresponding to the co-moving coordinate system before and after deformation, respectively.

The S-R decomposition theorem [40–44] states the following decomposition of deformation gradient F into the strain tensor and rotation tensor:

$$F = S + R \tag{1}$$

where the strain tensor is defined by

$$S_j^i = \frac{1}{2}(u^i|_j + u^i|_j^T) - L_k^i L_j^k (1 - \cos\theta) \tag{2}$$

and the rotation tensor is

$$R_j^i = \delta_j^i + L_j^i \sin\theta + L_k^i L_j^k (1 - \cos\theta) \tag{3}$$

where δ_j^i is the Kronecker-delta. In Eqs. (2) and (3), L_j^i is defined by

$$L_j^i = \frac{1}{2\sin\theta}(u^i|_j - u^i|_j^T) \tag{4}$$

and the average rotation angle θ is determined according to

$$\sin\theta = \frac{1}{2}\sqrt{(u^1|_2 - u^1|_2^T)^2 + (u^2|_3 - u^2|_3^T)^2 + (u^3|_1 - u^3|_1^T)^2} \tag{5}$$

The rotation in a deformed body can be generally described by three methods: (1) the coordinate axis method, i.e., according to [45] (figure 16.1 therein); (2) the quaternion method [46–48]; and (3) the axis-angle method [45,49]. In this study, a rotation matrix or tensor is expressed through a unit rotation axis vector (p) and a rotation angle (α) about the axis. For a rigid body rotation, the average rotation angle (θ) in the S-R decomposition is exactly the rotation angle (α) [40]. For the rotation of deformable body, the average rotation angle has a more profound meaning. Several typical examples were given by [40] to

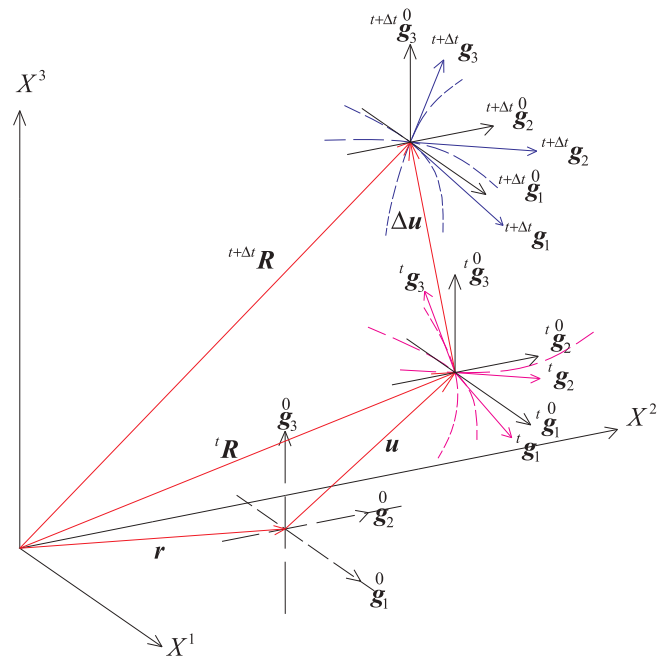


Fig. 2. Update of the three-dimension co-moving coordinate.

illustrate the features of the average rotation angle.

An updated co-moving coordinate as shown in Fig. 2 is adopted, where the superscript “ t ” and “ $t + \Delta t$ ” correspond to the two consecutive time t and $t + \Delta t$, respectively. In S-R decomposition theorem [43], the symmetric stress is work-conjugate to the strain defined by Eq. (2). Considering a deformable body and applying the principle of virtual displacement, the incremental governing equation can be expressed as [21]

$$\int_{t\Omega} \bar{\sigma}_j^i \delta(\Delta \bar{S}_{Li}^j + \Delta \bar{S}_{Ni}^j) d\Omega + \int_{t\Omega} \bar{D}_{jl}^{ik} (\Delta \bar{S}_{Lk}^l + \Delta \bar{S}_{Nk}^l) \delta(\Delta \bar{S}_{Li}^j + \Delta \bar{S}_{Ni}^j) d\Omega + \bar{F}_{ine} + \bar{F}_{pen} - \bar{F}_{ext} = 0 \tag{6}$$

where $\bar{\sigma}_j^i$ is the stress, $\Delta \bar{S}_{Li}^j$ and $\Delta \bar{S}_{Ni}^j$ are the linear and nonlinear strain increments, respectively. \bar{D}_{jl}^{ik} is the material tensor associated with the rate-form constitutive laws. Moreover \bar{F}_{ine} and \bar{F}_{pen} are the virtual work corresponding to the inertia force, constraint force of specified displacement, respectively. \bar{F}_{ext} represents the external force including the surface and body forces. The hat-lines “ $-$ ” and “ $=$ ” indicate that the variable with respect to basic vectors g_i^0 and $g_i^{t+\Delta t}$, respectively. For more details one can refer to [21].

The two-dimension problem has been addressed in [21], the three-dimension discretization format will be deduced here. For discretization of space domain, the same interpolation matrix $N(x,y,z)$ can be employed for expressing displacement u , velocity V and acceleration A . It should be pointed out that the expressions of $N(x,y,z)$ is dependent on the specific numerical method and the mesh topology.

Consider an arbitrary discrete unit, the displacement and displacement increment vectors related to the discrete unit can be denoted by u and Δu , respectively. Reconsidering Eq. (2), at any point in the discrete unit, the strain vector S can be written as

$$S(x,y,z) = \begin{pmatrix} S_1^1 \\ S_2^2 \\ S_3^3 \\ 2S_2^3 \\ 2S_1^3 \\ 2S_1^2 \end{pmatrix} = S_L + S_N = \begin{pmatrix} u^1|_1 \\ u^2|_2 \\ u^3|_3 \\ u^2|_3 + u^3|_2 \\ u^3|_1 + u^1|_3 \\ u^1|_2 + u^2|_1 \end{pmatrix} + \begin{pmatrix} -L_k^1 L_1^k (1 - \cos\theta) \\ -L_k^2 L_2^k (1 - \cos\theta) \\ -L_k^3 L_3^k (1 - \cos\theta) \\ -2L_k^2 L_3^k (1 - \cos\theta) \\ -2L_k^3 L_1^k (1 - \cos\theta) \\ -2L_k^1 L_2^k (1 - \cos\theta) \end{pmatrix}, \quad k = 1,2,3 \tag{7}$$

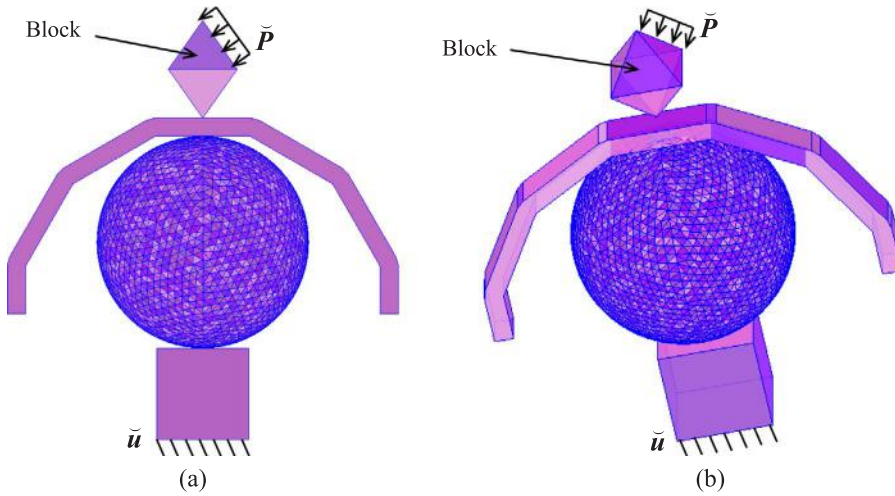


Fig. 3. An arbitrary block system. (a) 2D view; (b) 3D view.

The linear strain vector S_L can be expressed as

$$S_L(x,y,z) = \{u^1_1, u^2_2, u^3_3, u^2_3 + u^3_2, u^3_1 + u^1_3, u^1_2 + u^2_1\}^T = \mathbf{B}_L \mathbf{u}, \quad (8)$$

where the linear B-matrix \mathbf{B}_L is given by

$$\mathbf{B}_L = \begin{bmatrix} \frac{\partial}{\partial x} & 0 & 0 & 0 & \frac{\partial}{\partial z} & \frac{\partial}{\partial y} \\ 0 & \frac{\partial}{\partial y} & 0 & \frac{\partial}{\partial z} & 0 & \frac{\partial}{\partial x} \\ 0 & 0 & \frac{\partial}{\partial z} & \frac{\partial}{\partial y} & \frac{\partial}{\partial x} & 0 \end{bmatrix} \mathbf{N}(x,y,z). \quad (9)$$

If the following approximation

$$\cos\theta \approx 1 - \frac{1}{2}\theta^2$$

is used, the nonlinear strain vector S_N can be given by

$$S_N = - \begin{bmatrix} L_k^1 L_1^k (1 - \cos\theta) \\ L_k^2 L_2^k (1 - \cos\theta) \\ L_k^3 L_3^k (1 - \cos\theta) \\ 2L_k^2 L_3^k (1 - \cos\theta) \\ 2L_k^3 L_1^k (1 - \cos\theta) \\ 2L_k^1 L_2^k (1 - \cos\theta) \end{bmatrix} \approx \mathbf{B}_N \mathbf{u}. \quad (11)$$

By considering Eqs. (4), (5) and (10), the nonlinear B-matrix \mathbf{B}_N can be expressed by

$$\mathbf{B}_N = \begin{bmatrix} \frac{1}{8} \mathbf{L}_{N1} \mathbf{u} \mathbf{L}_{N1} + \frac{1}{8} \mathbf{L}_{N3} \mathbf{u} \mathbf{L}_{N3} \\ \frac{1}{8} \mathbf{L}_{N1} \mathbf{u} \mathbf{L}_{N1} + \frac{1}{8} \mathbf{L}_{N2} \mathbf{u} \mathbf{L}_{N2} \\ \frac{1}{8} \mathbf{L}_{N2} \mathbf{u} \mathbf{L}_{N2} + \frac{1}{8} \mathbf{L}_{N3} \mathbf{u} \mathbf{L}_{N3} \\ -\frac{1}{4} \mathbf{L}_{N1} \mathbf{u} \mathbf{L}_{N3} \\ -\frac{1}{4} \mathbf{L}_{N1} \mathbf{u} \mathbf{L}_{N2} \\ -\frac{1}{4} \mathbf{L}_{N2} \mathbf{u} \mathbf{L}_{N3} \end{bmatrix} = \frac{1}{8} \begin{bmatrix} \mathbf{L}_{N1} \mathbf{u} \mathbf{L}_{N1} + \mathbf{L}_{N3} \mathbf{u} \mathbf{L}_{N3} \\ \mathbf{L}_{N1} \mathbf{u} \mathbf{L}_{N1} + \mathbf{L}_{N2} \mathbf{u} \mathbf{L}_{N2} \\ \mathbf{L}_{N2} \mathbf{u} \mathbf{L}_{N2} + \mathbf{L}_{N3} \mathbf{u} \mathbf{L}_{N3} \\ -2\mathbf{L}_{N1} \mathbf{u} \mathbf{L}_{N3} \\ -2\mathbf{L}_{N1} \mathbf{u} \mathbf{L}_{N2} \\ -2\mathbf{L}_{N2} \mathbf{u} \mathbf{L}_{N3} \end{bmatrix} \quad (12)$$

where

$$\mathbf{L}_{N1} = \left[\frac{\partial}{\partial y}, -\frac{\partial}{\partial x}, 0 \right] \mathbf{N}(x,y,z), \quad (13)$$

$$\mathbf{L}_{N2} = \left[0, \frac{\partial}{\partial z}, -\frac{\partial}{\partial y} \right] \mathbf{N}(x,y,z), \quad (14)$$

$$\mathbf{L}_{N3} = \left[-\frac{\partial}{\partial z}, 0, \frac{\partial}{\partial x} \right] \mathbf{N}(x,y,z). \quad (15)$$

For the strain increment, the following variant of Eq. (12) can be employed.

$$\tilde{\mathbf{B}}_N = \frac{1}{8} \begin{bmatrix} \mathbf{L}_{N1} \Delta \mathbf{u}^* \mathbf{L}_{N1} + \mathbf{L}_{N3} \Delta \mathbf{u}^* \mathbf{L}_{N3} \\ \mathbf{L}_{N1} \Delta \mathbf{u}^* \mathbf{L}_{N1} + \mathbf{L}_{N2} \Delta \mathbf{u}^* \mathbf{L}_{N2} \\ \mathbf{L}_{N2} \Delta \mathbf{u}^* \mathbf{L}_{N2} + \mathbf{L}_{N3} \Delta \mathbf{u}^* \mathbf{L}_{N3} \\ -2\mathbf{L}_{N1} \Delta \mathbf{u}^* \mathbf{L}_{N3} \\ -2\mathbf{L}_{N1} \Delta \mathbf{u}^* \mathbf{L}_{N2} \\ -2\mathbf{L}_{N2} \Delta \mathbf{u}^* \mathbf{L}_{N3} \end{bmatrix} \quad (16)$$

where $\Delta \mathbf{u}^*$ is the displacement increment of the discrete unit corresponding to the previous calculation step. The effectiveness of Eq. (16) will be verified in Section 4. Therefore, the strain increment vectors ΔS_L and ΔS_N can be written as

$$\begin{aligned} \Delta S_L(x,y,z) &= \mathbf{B}_L \Delta \mathbf{u} \\ \Delta S_N(x,y,z) &= \tilde{\mathbf{B}}_N \Delta \mathbf{u} \end{aligned} \quad (17)$$

Noticing the arbitrariness of $\delta(\Delta \mathbf{u})$, Eq. (6) can be expressed by the following matrix format:

$$\mathbf{K} \Delta \mathbf{u} + \underbrace{\int_{t\Omega} \rho \mathbf{N}^T \mathbf{N} d\Omega}_{\text{Dynamic terms}} = \mathbf{F}_{\text{ext}} - \mathbf{F}_{\text{pen}} - \int_{t\Omega} (\mathbf{B}_L + \tilde{\mathbf{B}}_N)^T \boldsymbol{\sigma} d\Omega, \quad (18)$$

where

$$\begin{aligned} \mathbf{K} &= \int_{t\Omega} \mathbf{B}_L^T \mathbf{D} \mathbf{B}_L d\Omega + \int_{t\Omega} \mathbf{B}_L^T \mathbf{D} \tilde{\mathbf{B}}_N d\Omega + \int_{t\Omega} \tilde{\mathbf{B}}_N^T \mathbf{D} \mathbf{B}_L d\Omega \\ &\quad + \int_{t\Omega} \tilde{\mathbf{B}}_N^T \mathbf{D} \tilde{\mathbf{B}}_N d\Omega, \end{aligned} \quad (19)$$

where \mathbf{K} and \mathbf{D} are the stiffness matrix and material matrix, respectively. And

$$\mathbf{F}_{\text{pen}} = \int_{t\Gamma_u} \mathbf{N}^T \mathbf{k} (\mathbf{N} \Delta \mathbf{u} - \Delta \tilde{\mathbf{u}}) dS, \quad (20)$$

$$\mathbf{F}_{\text{ext}} = \int_{t\Gamma_P} \mathbf{N}^T \tilde{\mathbf{P}} dS + \int_{t\Omega} \rho \mathbf{N}^T \mathbf{f} d\Omega, \quad (21)$$

where $\Delta \tilde{\mathbf{u}}$ and $\tilde{\mathbf{P}}$ are the specified displacement and specified traction of any point on the boundary of the discrete unit, respectively. \mathbf{f} is the force per unit volume of the discrete unit. The penalty matrix \mathbf{k} is

$$\mathbf{k} = \begin{bmatrix} k^x & 0 & 0 \\ 0 & k^y & 0 \\ 0 & 0 & k^z \end{bmatrix}. \quad (22)$$

In this paper, the generalized- α method [50] is employed to discretize the time domain. For more detail one can refer to [21]. It should be noted that Eq. (17) is only used to treat the governing equation. Actually, the strain increment is given by

$$\Delta S_j^i = \frac{1}{2} (\Delta u^i_j + \Delta u^i_j{}^T) - \Delta L_k^i \Delta L_j^k (1 - \cos(\Delta\theta)), \quad (23)$$

where

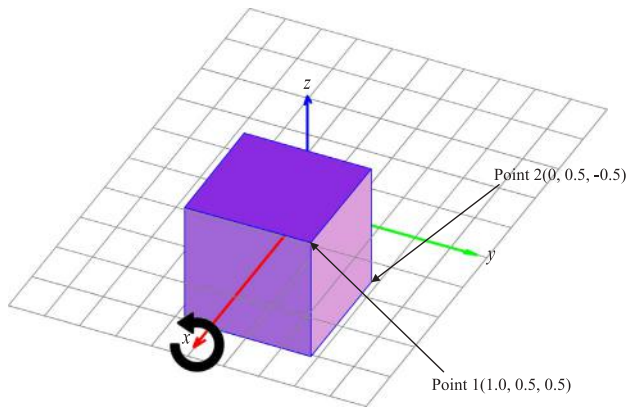


Fig. 4. Configuration of a cube rotating around x-axis.

$$\Delta L_j^i = \frac{1}{2\sin(\Delta\theta)}(\Delta u^i_j - \Delta u^i_j{}^T), \tag{24}$$

and

$$\sin(\Delta\theta) = \frac{1}{2}\sqrt{(\Delta u^1_2 - \Delta u^1_2{}^T)^2 + (\Delta u^2_3 - \Delta u^2_3{}^T)^2 + (\Delta u^1_3 - \Delta u^1_3{}^T)^2}. \tag{25}$$

Up to now, through the principle of virtual displacement the three-dimensional dynamic analysis formulation has been proposed on the basis of the S-R decomposition theorem. It is worth mentioning that the geometry of discrete unit has not yet been concretized. In other words, discrete unit may be the element or block or material point that depends on the specific numerical method. Therefore, the above equations are general and can be employed by any numerical methods, such as finite element method, numerical manifold method or meshless method. We consider only geometric nonlinearity similar to [21].

3. SR-3D-DDA

In this section, we will apply the above general formulation of dynamic analysis into DDA in order to establish a new approach termed as SR-3D-DDA, in which the discrete unit is embodied as the discrete block that can have arbitrary shapes, as shown in Fig. 3, where we consider a block “b”.

According to the theory of the 3D-DDA [23], the interpolation

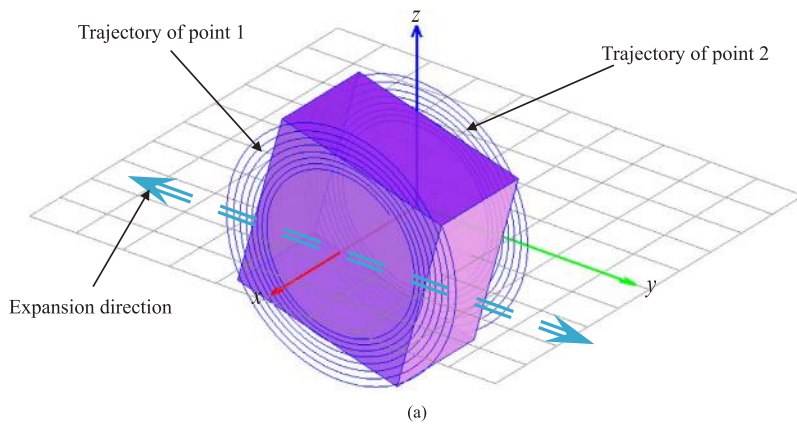
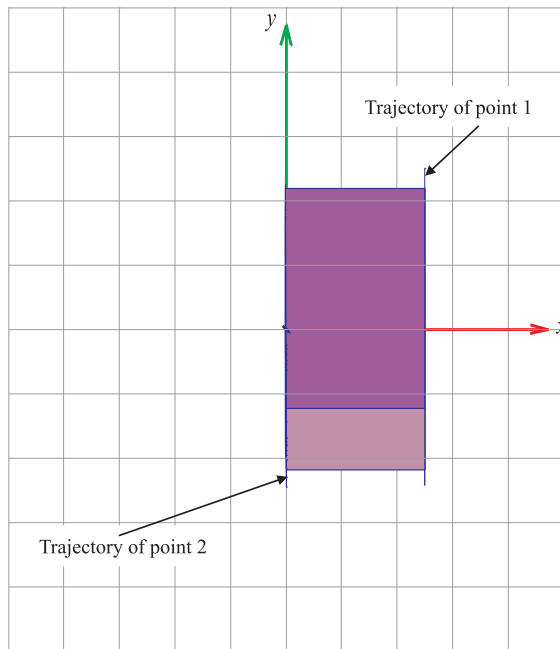


Fig. 5. Cube and the trajectories of CPs for rotating around x-axis: (a) 3D view predicted by DDA⁰, (b) 2D view predicted by DDA⁰, (c) 3D view predicted by DDA¹, (d) 2D view predicted by DDA¹; (e) 3D view predicted by DDA^{*} and (f) 2D view predicted by DDA^{*}.



(b)

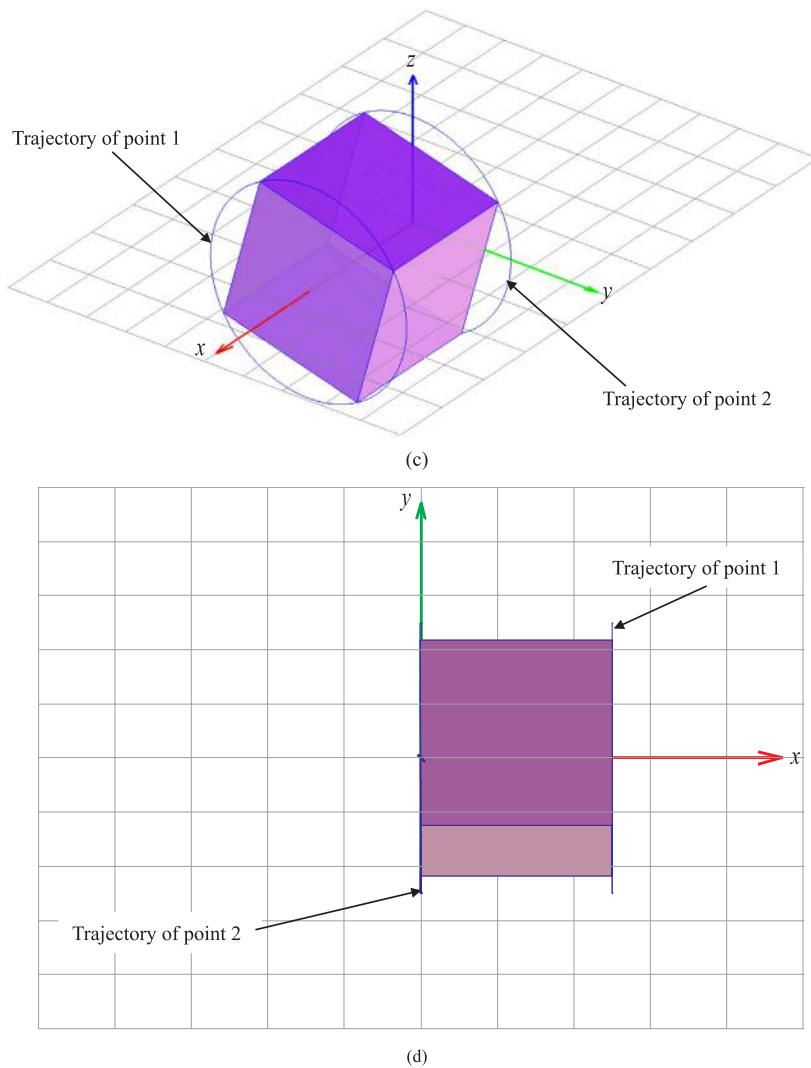


Fig. 5. (continued)

matrix can be given by

$$T(x,y,z) = \begin{bmatrix} 1 & 0 & 0 & 0 & z-z_c & y_c-y & x-x_c & 0 & 0 & 0 & 0 & (z-z_c)/2 & (y-y_c)/2 \\ 0 & 1 & 0 & z_c-z & 0 & x-x_c & 0 & y-y_c & 0 & (z-z_c)/2 & 0 & (x-x_c)/2 & 0 \\ 0 & 0 & 1 & y-y_c & x_c-x & 0 & 0 & 0 & z-z_c & (y-y_c)/2 & (x-x_c)/2 & 0 & 0 \end{bmatrix},$$

where (x_c, y_c, z_c) is the coordinates of the centroid of the block “b”. Further, for an any point in the block “b”, the displacement $\mathbf{u}(x,y,z)$ and displacement increment $\Delta\mathbf{u}(x,y,z)$ can be expressed by

$$\mathbf{u}(x,y,z) = \begin{pmatrix} u(x,y,z) \\ v(x,y,z) \\ w(x,y,z) \end{pmatrix} = \mathbf{T}(x,y,z)\mathbf{u}_b, \tag{27}$$

$$\Delta\mathbf{u}(x,y,z) = \begin{pmatrix} \Delta u(x,y,z) \\ \Delta v(x,y,z) \\ \Delta w(x,y,z) \end{pmatrix} = \mathbf{T}(x,y,z)\Delta\mathbf{u}_b, \tag{28}$$

where \mathbf{u}_b and $\Delta\mathbf{u}_b$ are the displacement vector and displacement increment vector of the block “b”, respectively. They can be written as

$$\mathbf{u}_b = (u_c, v_c, w_c, r_x, r_y, r_z, \varepsilon_x, \varepsilon_y, \varepsilon_z, \gamma_{yz}, \gamma_{zx}, \gamma_{xy}), \tag{29}$$

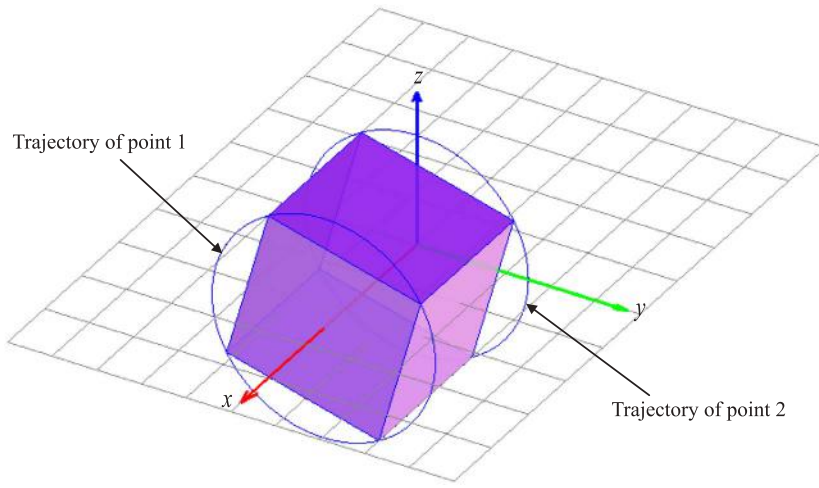
$$\Delta\mathbf{u}_b = (\Delta u_c, \Delta v_c, \Delta w_c, \Delta r_x, \Delta r_y, \Delta r_z, \Delta \varepsilon_x, \Delta \varepsilon_y, \Delta \varepsilon_z, \Delta \gamma_{yz}, \Delta \gamma_{zx}, \Delta \gamma_{xy}), \tag{30}$$

where u_c, v_c and w_c are the three translation components of the centroid of the block “b”; accordingly, $\Delta u_c, \Delta v_c$ and Δw_c are the increments of three translation components. r_x, r_y and r_z are the rigid-body rotation angles of the block “b” around x -, y - and z -axis, respectively. Thus, $\Delta r_x, \Delta r_y$ and Δr_z represent the corresponding rigid-body rotation angle increments. Moreover, $\varepsilon_x, \varepsilon_y, \varepsilon_z, \gamma_{yz}, \gamma_{zx}, \gamma_{xy}$ and $\Delta \varepsilon_x, \Delta \varepsilon_y, \Delta \varepsilon_z, \Delta \gamma_{yz}, \Delta \gamma_{zx}, \Delta \gamma_{xy}$ are the six strain components and the increments of the six strain components, respectively. In addition, the displacement increment of the block “b” corresponding to the previous calculation step is

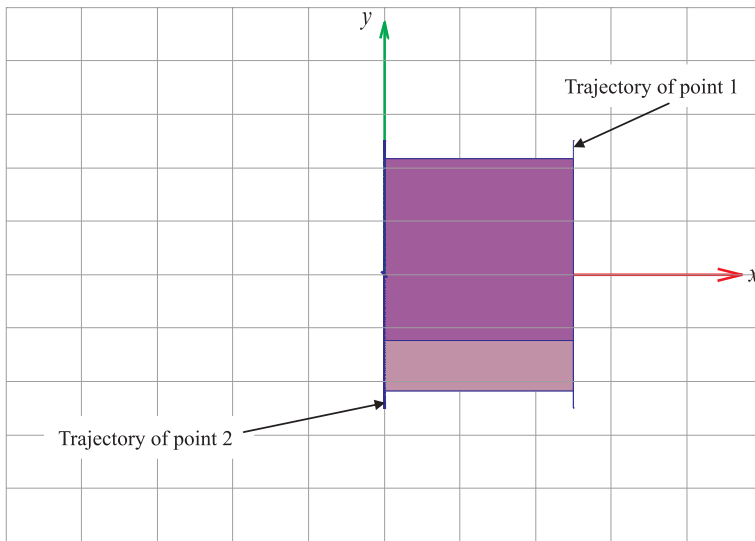
$$\Delta\mathbf{u}_b^* = (\Delta u_c^*, \Delta v_c^*, \Delta w_c^*, \Delta r_x^*, \Delta r_y^*, \Delta r_z^*, \Delta \varepsilon_x^*, \Delta \varepsilon_y^*, \Delta \varepsilon_z^*, \Delta \gamma_{yz}^*, \Delta \gamma_{zx}^*, \Delta \gamma_{xy}^*). \tag{31}$$

Further, corresponding to the block “b”, the linear B-matrix

Fig. 5. (continued)



(e)



(f)

becomes

$$B_{bL} = \begin{bmatrix} 0 & 0 & 0 & 0 & 0 & 0 & 1 & 0 & 0 & 0 & 0 & 0 \\ 0 & 0 & 0 & 0 & 0 & 0 & 0 & 1 & 0 & 0 & 0 & 0 \\ 0 & 0 & 0 & 0 & 0 & 0 & 0 & 0 & 1 & 0 & 0 & 0 \\ 0 & 0 & 0 & 0 & 0 & 0 & 0 & 0 & 0 & 1 & 0 & 0 \\ 0 & 0 & 0 & 0 & 0 & 0 & 0 & 0 & 0 & 0 & 1 & 0 \\ 0 & 0 & 0 & 0 & 0 & 0 & 0 & 0 & 0 & 0 & 0 & 1 \end{bmatrix} \quad (32)$$

And the variant of nonlinear B-matrix reads

$$\tilde{B}_{bN} = \begin{bmatrix} 0 & 0 & 0 & 0 & \frac{\Delta r_y^*}{2} & \frac{\Delta r_z^*}{2} & 0 & 0 & 0 & 0 & 0 & 0 \\ 0 & 0 & 0 & \frac{\Delta r_x^*}{2} & 0 & \frac{\Delta r_z^*}{2} & 0 & 0 & 0 & 0 & 0 & 0 \\ 0 & 0 & 0 & \frac{\Delta r_x^*}{2} & \frac{\Delta r_y^*}{2} & 0 & 0 & 0 & 0 & 0 & 0 & 0 \\ 0 & 0 & 0 & 0 & -\Delta r_z^* & 0 & 0 & 0 & 0 & 0 & 0 & 0 \\ 0 & 0 & 0 & -\Delta r_z^* & 0 & 0 & 0 & 0 & 0 & 0 & 0 & 0 \\ 0 & 0 & 0 & 0 & -\Delta r_x^* & 0 & 0 & 0 & 0 & 0 & 0 & 0 \end{bmatrix} \quad (33)$$

The material matrix D given by

Table 1
Volume of a cube corresponding to single-axial rotation.

Time (CS)	DDA ⁰		DDA ¹		DDA [*]	
	CV (m ³)	ER (%)	CV (m ³)	ER (%)	CV (m ³)	ER (%)
100	1.0408	4.0802	1.0000	0.0000	1.0000	0.0000
200	1.0833	8.3270	1.0000	0.0000	1.0000	0.0000
500	1.2214	22.1354	1.0000	0.0000	1.0000	0.0000
1000	1.4917	49.1706	1.0000	0.0000	1.0000	0.0000
2500	2.7177	171.7739	1.0000	0.0000	1.0000	0.0000

Analytical solution: Volume = 1.0000 m³.
(CS: calculation step, CV: calculation value, RE: relative error).

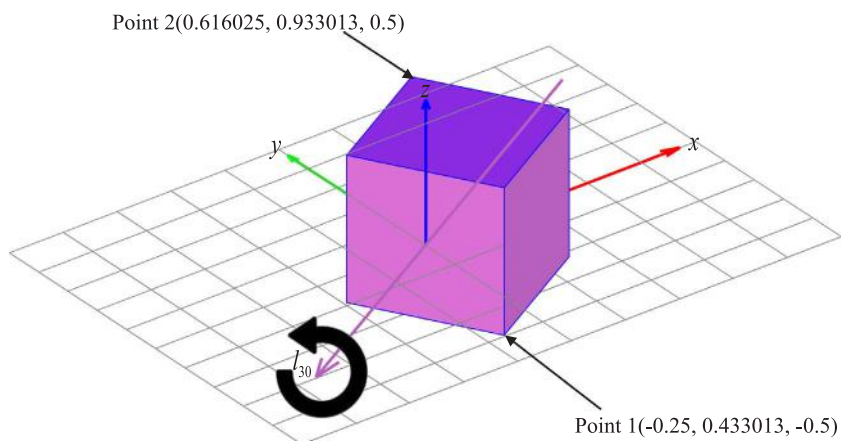


Fig. 6. Configuration of a cube rotating around l_{30} -axis.

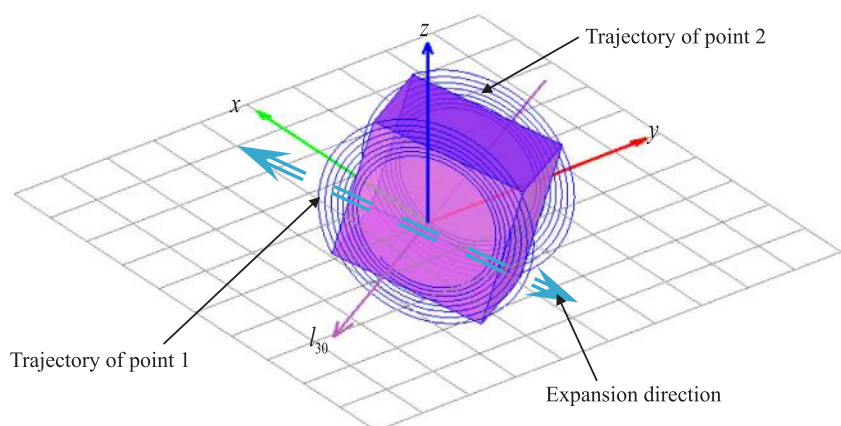
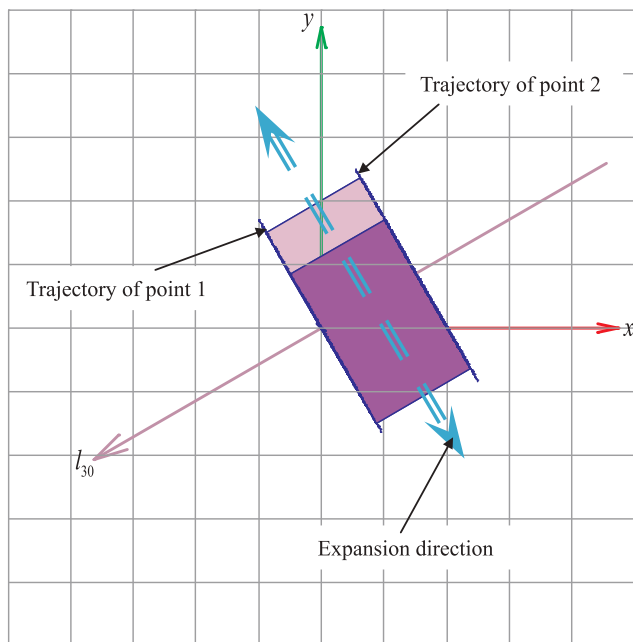


Fig. 7. Cube and the trajectories of CPs for rotating around l_{30} -axis:(a) 3D view predicted by DDA^0 , (b) 2D view predicted by DDA^0 , (c) 3D view predicted by DDA^1 , (d) 2D view predicted by DDA^1 ; (e) 3D view predicted by DDA^* and (f) 2D view predicted by DDA^* .

(a)



(b)

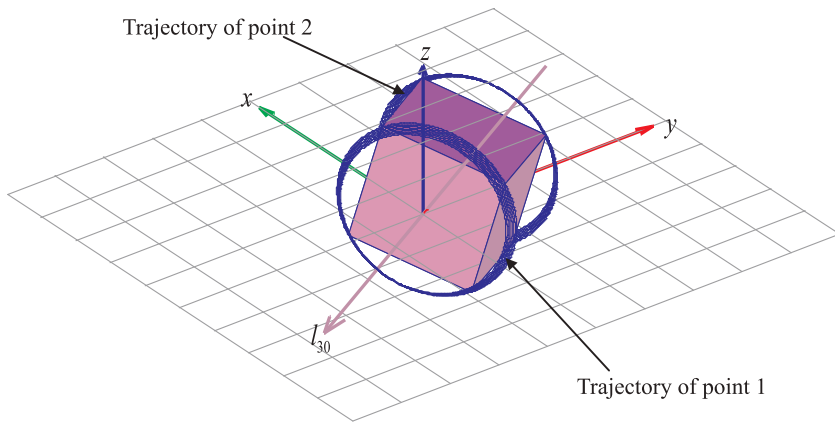
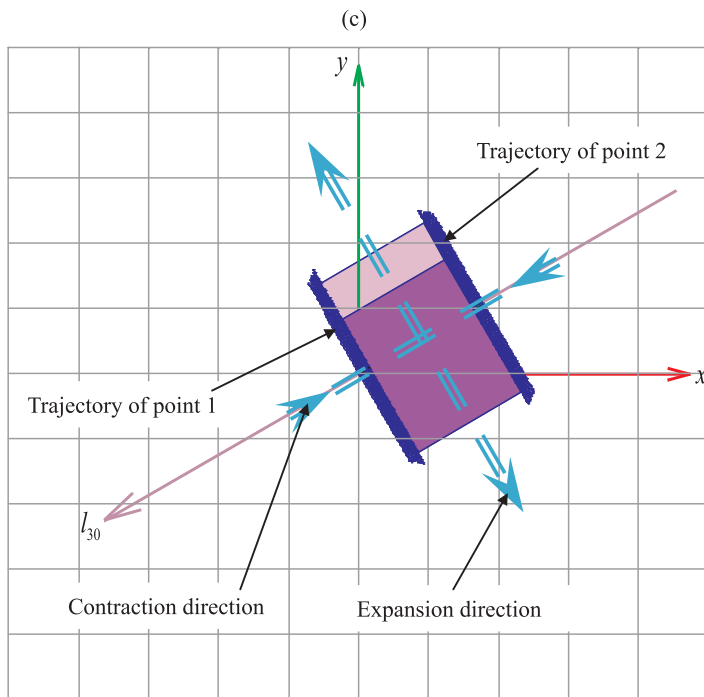


Fig. 7. (continued)



(d)

$$\mathbf{D} = \frac{E}{(1+\nu)(1-2\nu)} \begin{bmatrix} 0 & 0 & 0 & 0 & 0 & 0 & 0 & 0 & 0 & 0 & 0 \\ 0 & 0 & 0 & 0 & 0 & 0 & 0 & 0 & 0 & 0 & 0 \\ 0 & 0 & 0 & 0 & 0 & 0 & 0 & 0 & 0 & 0 & 0 \\ 0 & 0 & 0 & 0 & 0 & 0 & 0 & 0 & 0 & 0 & 0 \\ 0 & 0 & 0 & 0 & 0 & 0 & 0 & 0 & 0 & 0 & 0 \\ 0 & 0 & 0 & 0 & 0 & 0 & 0 & 0 & 0 & 0 & 0 \\ 0 & 0 & 0 & 0 & 0 & 0 & 0 & 0 & 0 & 0 & 0 \\ 0 & 0 & 0 & 0 & 0 & 0 & 1-\nu & \nu & \nu & 0 & 0 \\ 0 & 0 & 0 & 0 & 0 & \nu & 1-\nu & \nu & 0 & 0 & 0 \\ 0 & 0 & 0 & 0 & 0 & \nu & \nu & 1-\nu & 0 & 0 & 0 \\ 0 & 0 & 0 & 0 & 0 & 0 & 0 & 0 & 1/2-\nu & 0 & 0 \\ 0 & 0 & 0 & 0 & 0 & 0 & 0 & 0 & 0 & 1/2-\nu & 0 \\ 0 & 0 & 0 & 0 & 0 & 0 & 0 & 0 & 0 & 0 & 1/2-\nu \end{bmatrix} \quad (34)$$

Substitution of Eq. (26), (32)–(34) into Eqs. (18)–(21) yields $(\mathbf{K}_b + \mathbf{M}_b)\Delta\mathbf{u}_b = \mathbf{F}_b$, (35)

where \mathbf{K}_b , \mathbf{M}_b and \mathbf{F}_b are the stiffness matrix, the mass matrix and the equivalent force vector of the block “b”, respectively. For detailed formulations on the matrix of normal contact, the matrices of shear contact and friction force, one can refer to [23] for more details. Once these matrices are obtained, the control equation of entire block system

can easily be formed, which furnishes the SR based 3D-DDA. For 2D-DDA [22], the interpolation matrix reduces to

$$\mathbf{T}(x,y) = \begin{bmatrix} 1 & 0 & y_c - y & x - x_c & 0 & \frac{y - y_c}{2} \\ 0 & 1 & x - x_c & 0 & y - y_c & \frac{x - x_c}{2} \end{bmatrix} \quad (36)$$

And $\Delta\mathbf{u}_b^*$ becomes

$$\Delta\mathbf{u}_b^* = (\Delta u_c^*, \Delta v_c^*, \Delta r_z^*, \Delta \epsilon_x^*, \Delta \epsilon_y^*, \Delta \gamma_{xy}^*). \quad (37)$$

Then, one can obtain

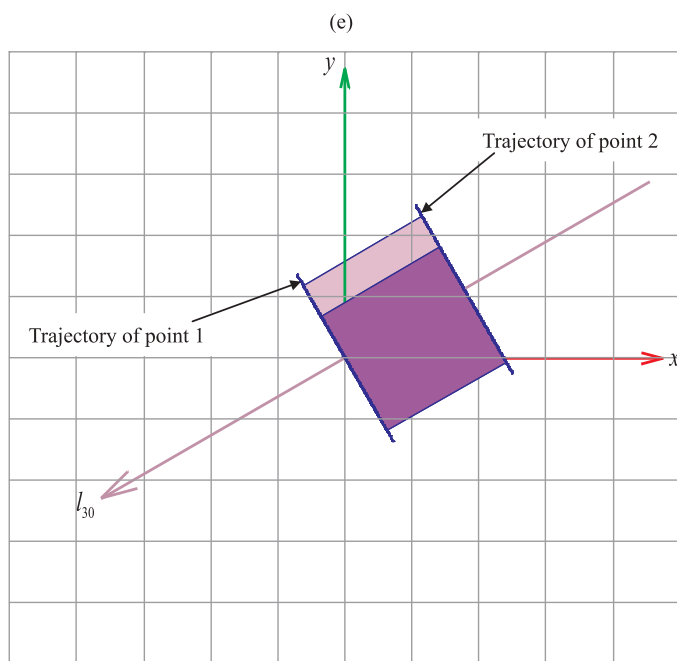
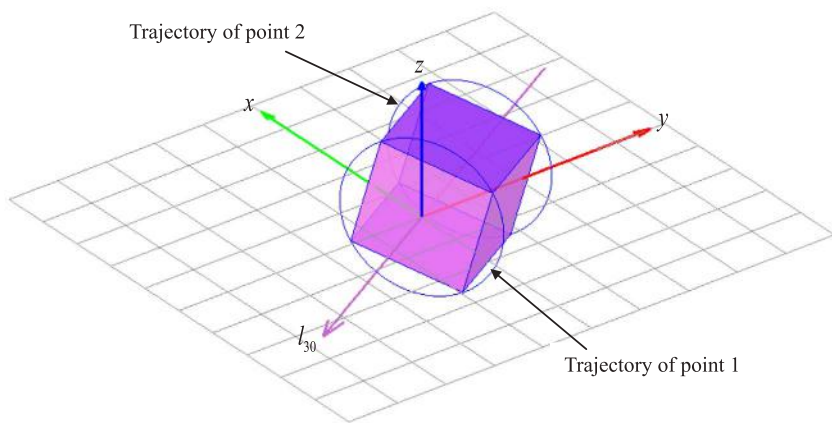
$$\mathbf{B}_{bL} = \begin{bmatrix} 0 & 0 & 0 & 1 & 0 & 0 \\ 0 & 0 & 0 & 0 & 1 & 0 \\ 0 & 0 & 0 & 0 & 0 & 1 \end{bmatrix}. \quad (38)$$

Referring to Eq. (66) in [21], we have

$$\tilde{\mathbf{B}}_{bN} = \begin{bmatrix} 0 & 0 & \Delta r_z^*/2 & 0 & 0 & 0 \\ 0 & 0 & \Delta r_z^*/2 & 0 & 0 & 0 \\ 0 & 0 & 0 & 0 & 0 & 0 \end{bmatrix}. \quad (39)$$

Moreover, the material matrix \mathbf{D} becomes

Fig. 7. (continued)



$$D = \frac{\bar{E}}{1-\bar{\nu}^2} \begin{bmatrix} 1 & \bar{\nu} & 0 \\ \bar{\nu} & 1 & 0 \\ 0 & 0 & (1-\bar{\nu})/2 \end{bmatrix} \tag{40}$$

For the plane stress problem $\bar{E} = E, \bar{\nu} = \nu$; while for the plane strain

Table 2
Volume of a cube corresponding to dual-axial rotation.

Time (CS)	DDA ⁰		DDA ¹		DDA [*]	
	CV (m ³)	ER (%)	CV (m ³)	ER (%)	CV (m ³)	ER (%)
100	1.0408	4.0802	1.0000	0.0000	1.0000	0.0000
200	1.0833	8.3270	1.0000	0.0000	1.0000	0.0000
500	1.2214	22.1354	1.0000	0.0000	1.0000	0.0000
1000	1.4917	49.1706	1.0000	0.0000	1.0000	0.0000
2500	2.7177	171.7739	1.0000	0.0000	1.0000	0.0000

Analytical solution: Volume = 1.0000 m³.
(CS: calculation step, CV: calculation value, RE: relative error).

problem $\bar{E} = E/(1-\nu^2), \bar{\nu} = \nu/(1-\nu)$, where E and ν are the Young's modulus and Poisson's ratio, respectively.

Through substituting Eqs. (36) and (38)–(40) into Eqs. (18)–(21) of [21], SR-2D-DDA can be achieved. SR-2D-DDA has been integrated into the modified 2D-DDA presented in [51].

The computational procedure can be summarized as follows:

- Step 1: Input geometry and material information.
- Step 2: Set initial values, let $\Delta u_b^* = \Delta u_b^0$, and construct B_{bL} by using Eq. (32).
- Step 3: Construct \tilde{B}_{bN} by using Eq. (33).
- Step 4: Generate the controlling equation by using Eqs. (18)–(21) and (35) and the generalized- α method [21].
- Step 5: Treat contact, and modify the controlling equation if necessary.
- Step 6: Solve the controlling equation to obtain Δu_b .
- Step 7: Conduct the open-close iteration until the convergence is reached.

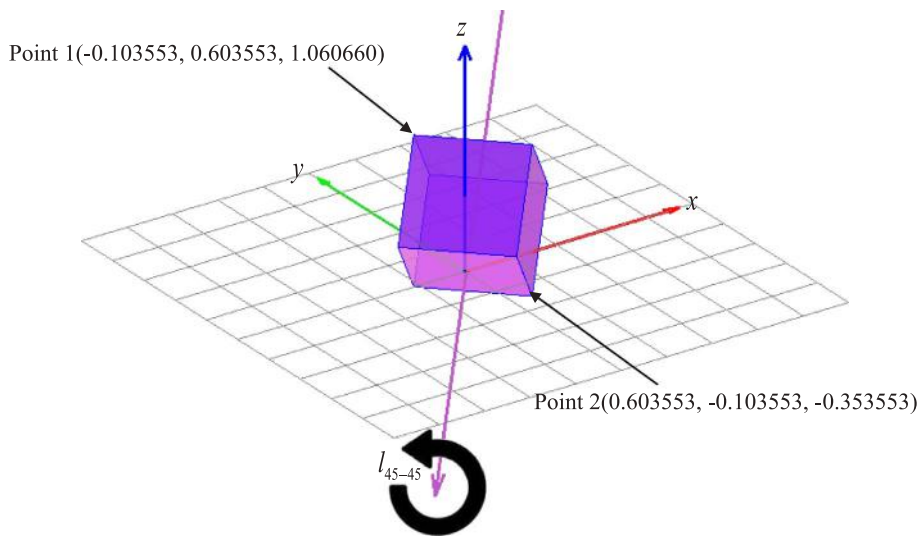


Fig. 8. Configuration of a cube rotating around l_{45-45} -axis.

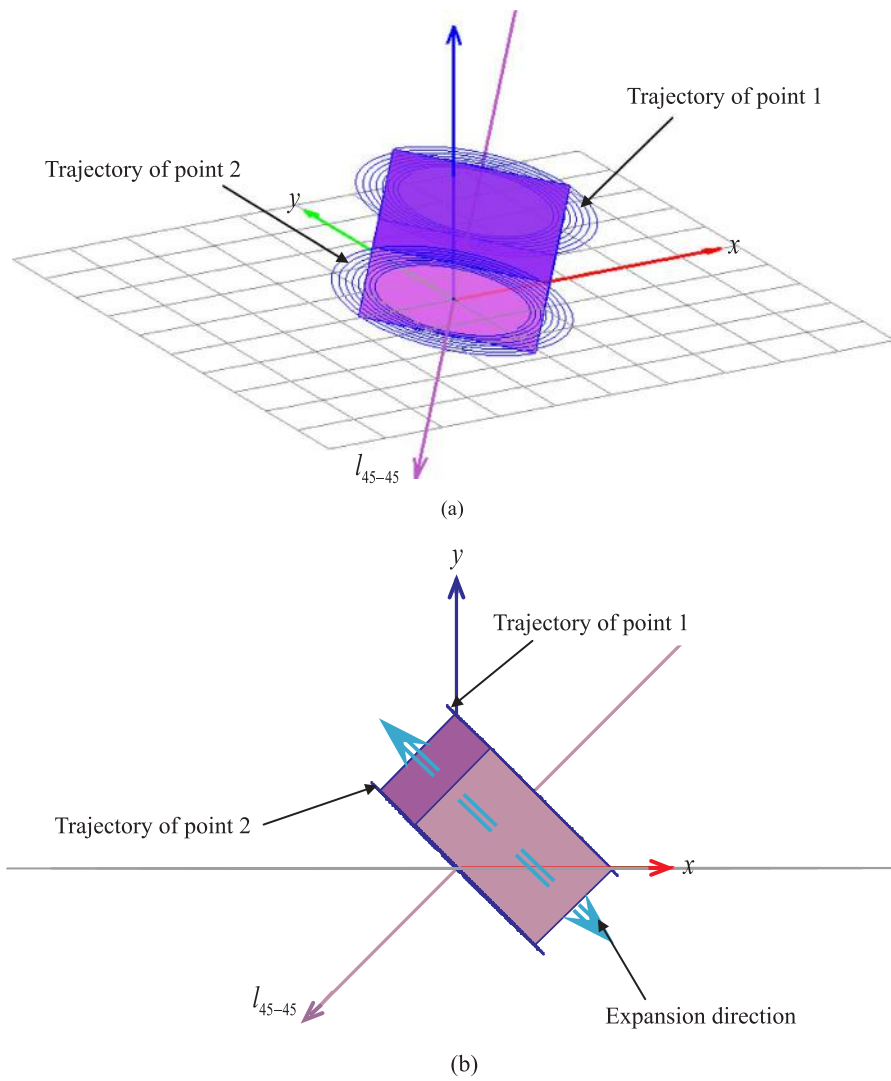
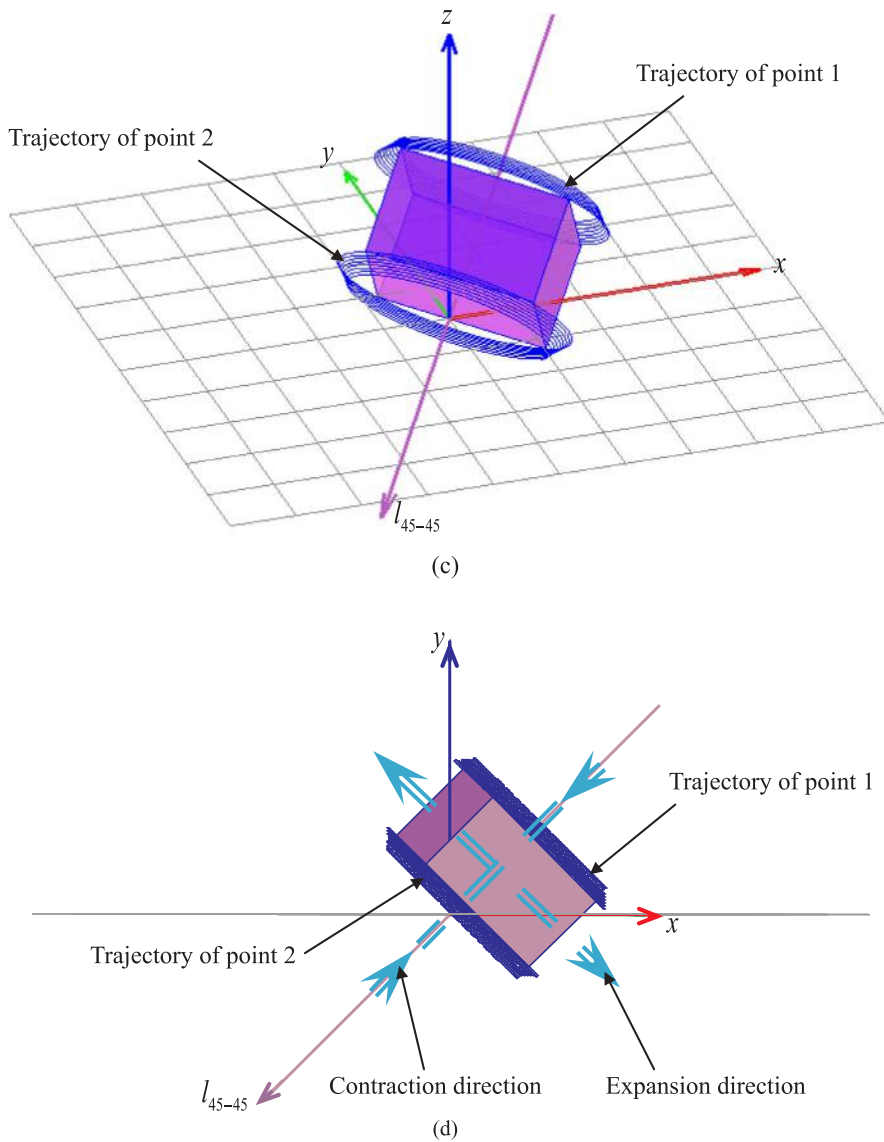


Fig. 9. Cube and the trajectories of CPs for rotating around l_{45-45} -axis: (a) 3D view predicted by DDA^0 , (b) 2D view predicted by DDA^0 , (c) 3D view predicted by DDA^1 , (d) 2D view predicted by DDA^1 ; (e) 3D view predicted by DDA^* and (f) 2D view predicted by DDA^* .

Fig. 9. (continued)



- Step 8: Compute the strain increment ΔS^j (Eqs. (23)–(25)) and the stress increment $\Delta \sigma^j$ by using the constitutive relation.
- Step 9: Update strain, stress, geometry, velocity and acceleration by using the Newmark method [52].
- Step 10: Let $\Delta u_b^* = \Delta u_b^0$ and repeat Step 3–9 until the total time is completed.

4. Numerical examples

In this section, several tests are provided to demonstrate the capability and advantage of the SR-3D-DDA. As is known, the three axis of Cartesian coordinate system may be the axis of rotation. Here, we will give three definitions: the first is “single-axial rotation”, which means that only one angular velocity is nonzero, i.e. $\omega_x \neq 0$ and $\omega_y = \omega_z = 0$ or $\omega_y \neq 0$ and $\omega_x = \omega_z = 0$, and so forth; the second is “dual-axial rotation”, which declares that there are two nonzero angular velocities, i.e. $\omega_x \neq 0, \omega_y \neq 0$ and $\omega_z = 0$ or $\omega_x \neq 0, \omega_z \neq 0$ and $\omega_y = 0$, and so on; the last is “tri-axial rotation”, which indicates that there are three nonzero angular velocities, namely $\omega_x \neq 0, \omega_y \neq 0$ and $\omega_z \neq 0$.

For the convenience of comparison, in this paper, DDA⁰ refers to the original formulation of DDA given by [23]; DDA¹ signifies that the

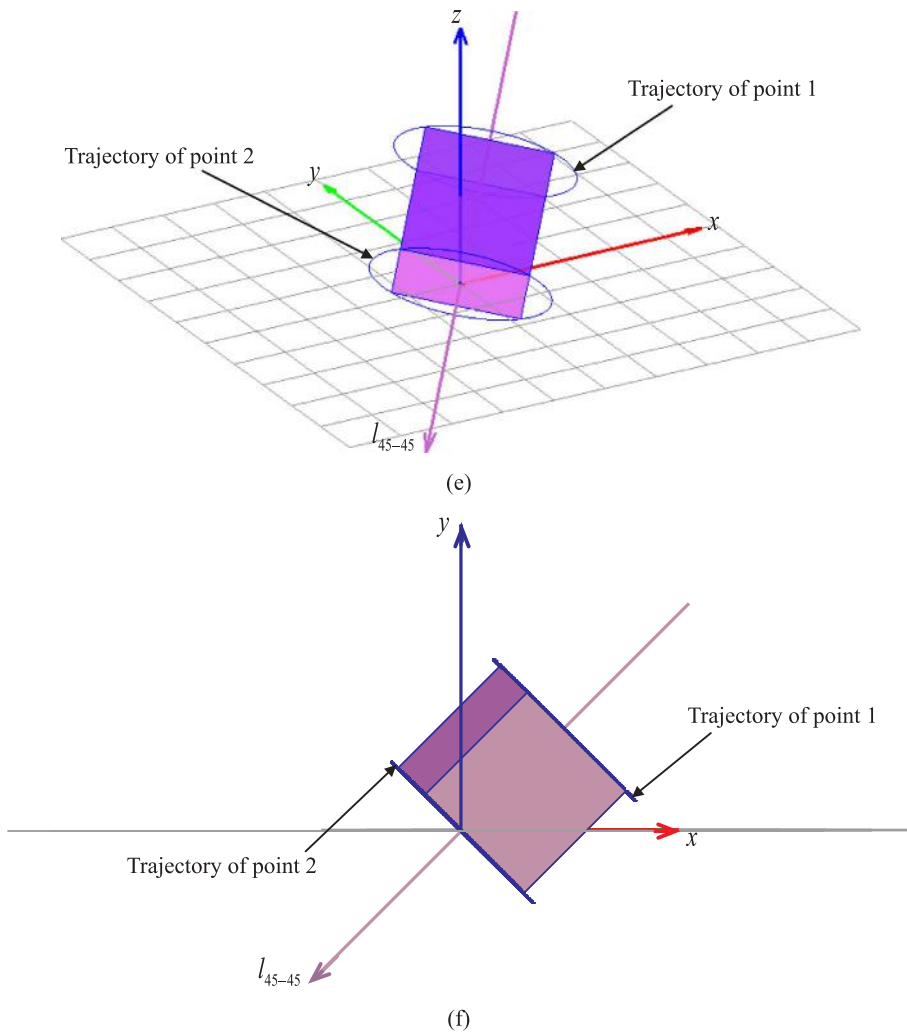
following 3D displacement adjustment method (Eq. (41)) [36] are adopted after solving the control equation to overcome the false volume expansion; and DDA^{*} stands for SR-3D-DDA.

$$\begin{aligned} \Delta u &= \Delta u_c + (x-x_c)(\cos\Delta r_z-1)-(y-y_c)\sin\Delta r_z \\ &\quad + (z-z_c)\sin\Delta r_y + (x-x_c)(\cos\Delta r_y-1) \\ \Delta v &= \Delta v_c + (x-x_c)\sin\Delta r_z + (y-y_c)(\cos\Delta r_z-1) \\ &\quad + (y-y_c)(\cos\Delta r_x-1)-(z-z_c)\sin\Delta r_x \\ \Delta w &= \Delta w_c + (z-z_c)(\cos\Delta r_y-1)-(x-x_c)\sin\Delta r_y \\ &\quad + (y-y_c)\sin\Delta r_x + (z-z_c)(\cos\Delta r_x-1) \end{aligned} \tag{41}$$

4.1. Single-axial rotation of a cube

The configuration of a cube (1 m × 1 m × 1 m) is shown in Fig. 4. Without loss of generality, we consider a single-axial rotation, and let the original rotation angular velocities to be $\omega_x = 2.00$ rad/s and $\omega_y = \omega_z = 0$, respectively. The cube will rotate anticlockwise around the x-axis. And points 1(0, 0.5, -0.5) and 2(1.0, 0.5, 0.5) are used as the two checking points, as shown in Fig. 4. Moreover, the material is assumed to be elastic and the density is $\rho = 2450$ kg/m³, Young’s Modulus is $E = 4.0 \times 10^9$ Pa, Poisson’s ratio is $\nu = 0.35$. The gravity is

Fig. 9. (continued)



not considered. The real time interval per calculation step (CS) is given by $\Delta = 0.01$ s; the total number of calculation step is $CS = 2500$; the spectral radius of the generalized- α method [50] is given by $\rho_\infty = 1$. The results obtained by DDA^0 , DDA^1 , and DDA^* are shown in Fig. 5.

For DDA^0 , as shown in Fig. 5(a), the expansion along the direction perpendicular to the axis of rotation is apparent, which results in outward offsets of trajectories of points 1 and 2, as shown in Fig. 5(a). On the other hand, the trajectories of points 1 and 2 appear to be the two line segments in Fig. 5(b), implying that nonphysical expansion or contraction does not occur in the direction parallel to the axis of rotation. Fig. 5(c) up to (f) present some results obtained by DDA^1 and DDA^* , respectively.

For DDA^1 , as we expected, the trajectories of points 1 and 2 are all the circles in the 3D view and they all look like a line segment in the 2D view, as shown in Fig. 5(c) and (d). For DDA^* , as shown in Fig. 5(e) and (f), the results are almost the same as that given by DDA^1 . In fact, for the case of the other two single-axial rotations, namely $\omega_y \neq 0$ and $\omega_x = \omega_z = 0$ or $\omega_z \neq 0$ and $\omega_x = \omega_y = 0$, our calculations indicate that neither expansion nor contraction does not exist in DDA^1 and DDA^* . In addition, Table 1 shows that the volume of the cube obtained by DDA^0 is increasingly enlarged, and DDA^1 and DDA^* can all offer correct values for the volume.

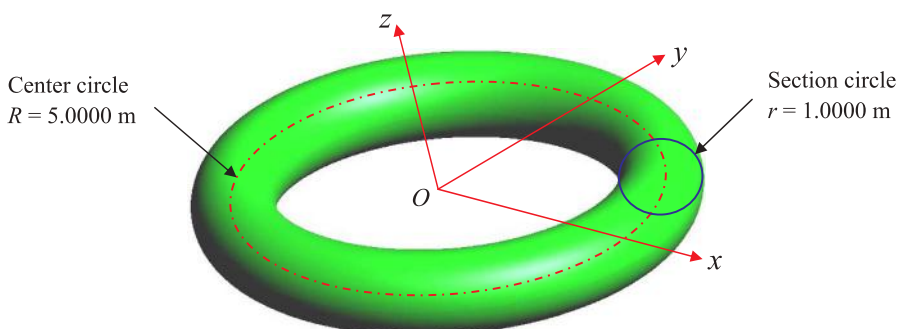


Fig. 10. Geometry of a torus.

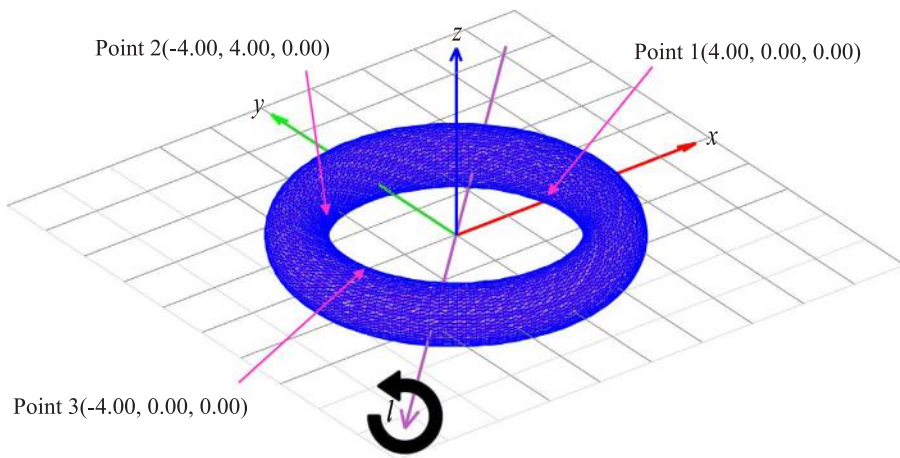


Fig. 11. Discrete model of a torus.

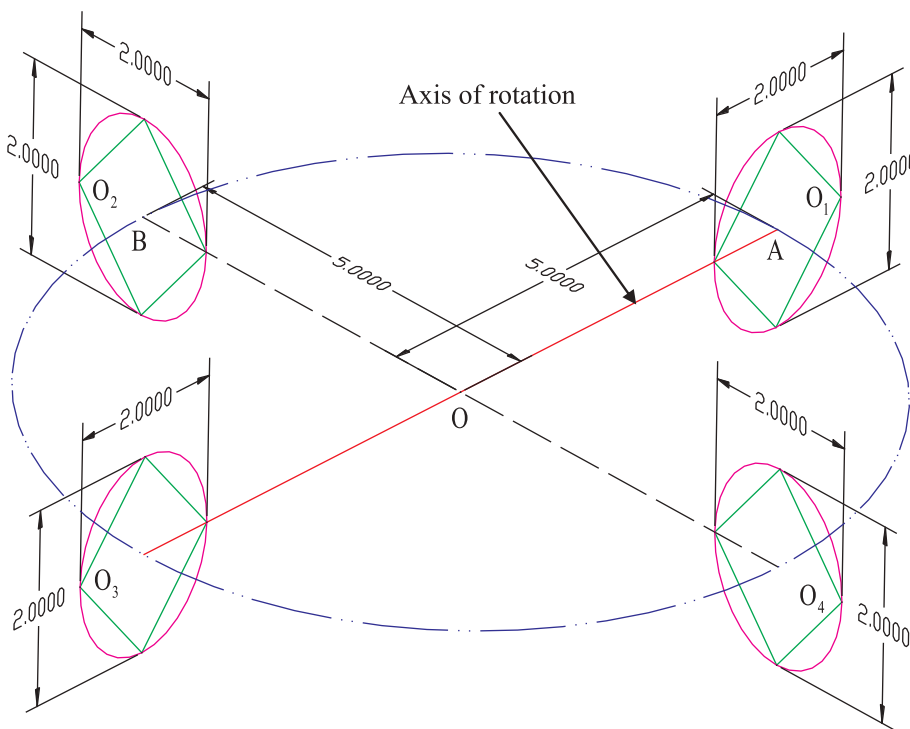


Fig. 12. Line segments OA and OB and sections O₁, O₂, O₃ and O₄ (CS = 0).

4.2. Dual-axial rotation of a cube

If $\omega_x = -1.7320508 \text{ rad/s}$, $\omega_y = -0.5 \text{ rad/s}$ and $\omega_z = 0$, the cube will rotate around l_{30} -axis, in which the subscript “30” means that the intersection angle between the axis of rotation and x-axis is equal to 30°. And points 1(-0.25, 0.433013, -0.5) and 2(0.616025, 0.933013, 0.5) serves as the checking points, as shown in Fig. 6. The results obtained by DDA⁰, DDA¹ and DDA* are shown in Fig. 7.

For DDA⁰, similar to the single-axial rotation, the expansion along the direction perpendicular to the axis of rotation is also apparent, leading to outward offsets of trajectories of points 1 and 2, as shown in Fig. 7(a). Moreover, for the two checking points, their trajectories are the two line segments in Fig. 7(b). There is neither expansion nor contraction in the direction parallel to the axis of rotation.

For DDA¹, unlike the single-axial rotation, in the direction perpendicular and parallel to l_{30} -axis the corresponding expansion and contraction can be identified easily, as shown in Fig. 7(c). Thus, the

trajectory of point 1 or 2 resembles a trapezoid in the 2D view, as shown in Fig. 7(d).

For DDA*, in the 3D view, the trajectories of points 1 and 2 are all the circles, as shown in Fig. 7(e), whereas in the 2D view, the trajectories of points 1 and 2 are all the line segments, as shown in Fig. 7(f). Therefore, we can conclude that neither expansion nor contraction exists in DDA* for dual-axial rotation.

In addition, we shown in Table 2 that the volume of the cube given by DDA⁰ is gradually expanded, and both DDA¹ and DDA* can obtain the correct results. It should be pointed out that DDA¹ cannot provide the shape of cube due to the nonphysical expansion and contraction, whilst that DDA* can guarantee the shape and volume of the cube are no change.

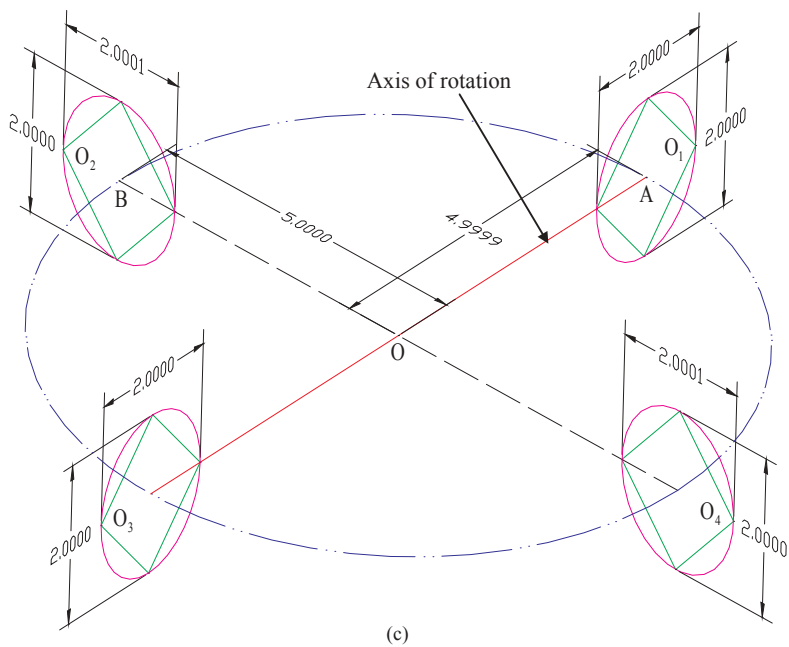
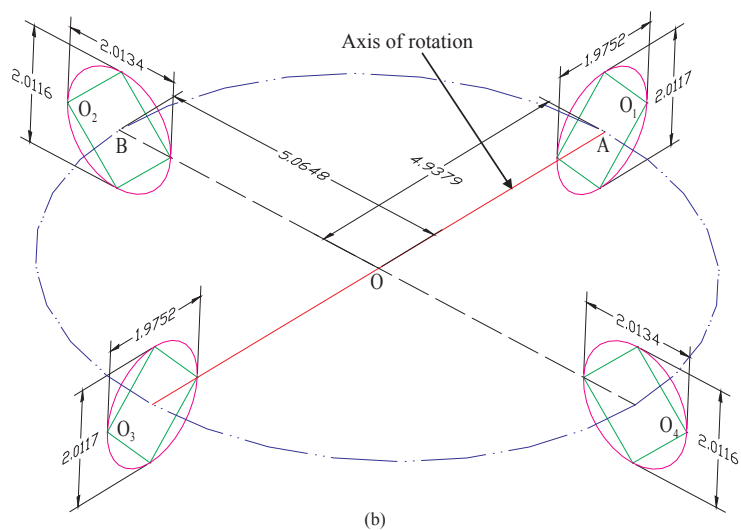
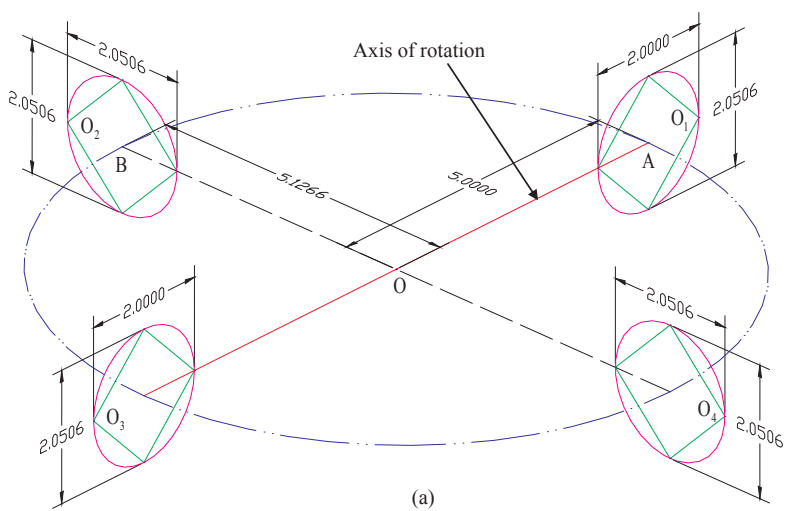


Fig. 13. Line segments OA and OB and sections O_1 , O_2 , O_3 and O_4 (CS = 1000): (a) Predicted by DDA^0 ; (b) Predicted by DDA^1 and (c) Predicted by DDA^* .

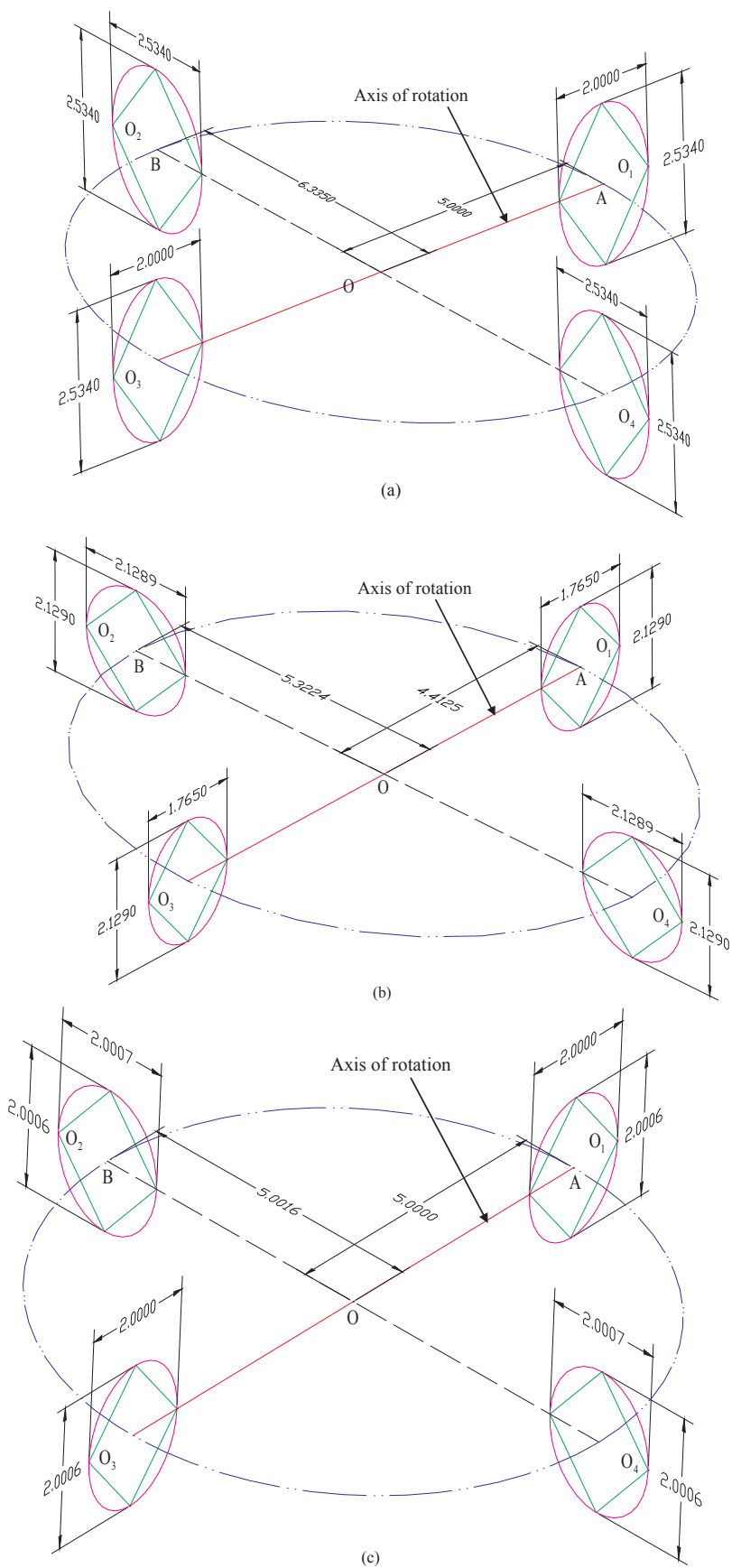


Fig. 14. Line segments OA and OB and sections O_1 , O_2 , O_3 and O_4 ($CS = 8000$). (a) Predicted by DDA^0 ; (b) Predicted by DDA^1 and (c) Predicted by DDA^* .

4.3. Tri-axial rotation of a cube

Now, we consider the example of a tri-axial rotation. First, we rotate the rotational axis of example1 (see Fig. 4) by 45° from x-axis to y-axis, and then allow a 45° inclined angle between the axis and the x-y plane, as shown in Fig. 8. Set the original rotation angular velocities to be $\omega_x = -1.00$ rad/s, $\omega_y = -1.00$ rad/s and $\omega_z = -1.414213$ rad/s, respectively. Therefore, the cube will rotate anticlockwise around the l_{45-45} -axis. Points 1(-0.103553, 0.603553, 1.060660) and 2(0.603553, -0.103553, -0.353553) are taken as the two checking points. The results obtained by DDA⁰, DDA¹ and DDA* are shown in Fig. 9.

For DDA⁰, from Fig. 9(a) and (b) we can know, similar to the single and dual-axial rotation cases, there is only an expansion in the direction perpendicular to the axis of rotation.

For DDA¹, like the dual-axial rotation (refer to Fig. 7(c) and (d)), there are an expansion in the direction perpendicular to the axis of rotation and a contraction in the direction parallel to the rotational axis, as shown in Fig. 9(c) and (d).

According to Figs. 5(e) and (f), 7(e) and (f) and 9(e) and (f), DDA* performs rather satisfactorily in all three cases of single, dual and tri-

axial rotations.

4.4. Dual-axial rotation of a torus

The geometry of a torus with the centerline radius $R = 5.0000$ m and the cross section radius $r = 1.0000$ m is considered. The center of the torus coincides with the origin of Cartesian coordinate system and the center circle is located on the x-y plane, as shown in Fig. 10.

The torus is firstly discretized into 13,104 triangular faces. These faces are closed on to form a 3-dimensional DDA block with a volume of 98.4153 m³, which is rather close to the analytical solution 98.6960 m³. In this example, we set the original rotation angular velocities to be $\omega_x = \omega_y = -5.00$ rad/s and $\omega_z = 0$, respectively. Thus, the torus will rotate anticlockwise around the l -axis. Points 1(4.00, 0.00, 0.00), 2(-4.00, 4.00, 0.00) and 3(-4.00, 0.00, 0.00) are chosen as checking points, as shown in Fig. 11. In addition, the material of the torus is assumed to be elastic and the density is $\rho = 2.500$ kg/m³, Young's Modulus is $E = 2.0 \times 10^9$ Pa, Poisson's ratio is $\nu = 0.25$. The gravity is ignored. Moreover, the real time interval per calculation step is given by $\Delta = 0.001$ s; the total number of calculation step is CS = 8000; the

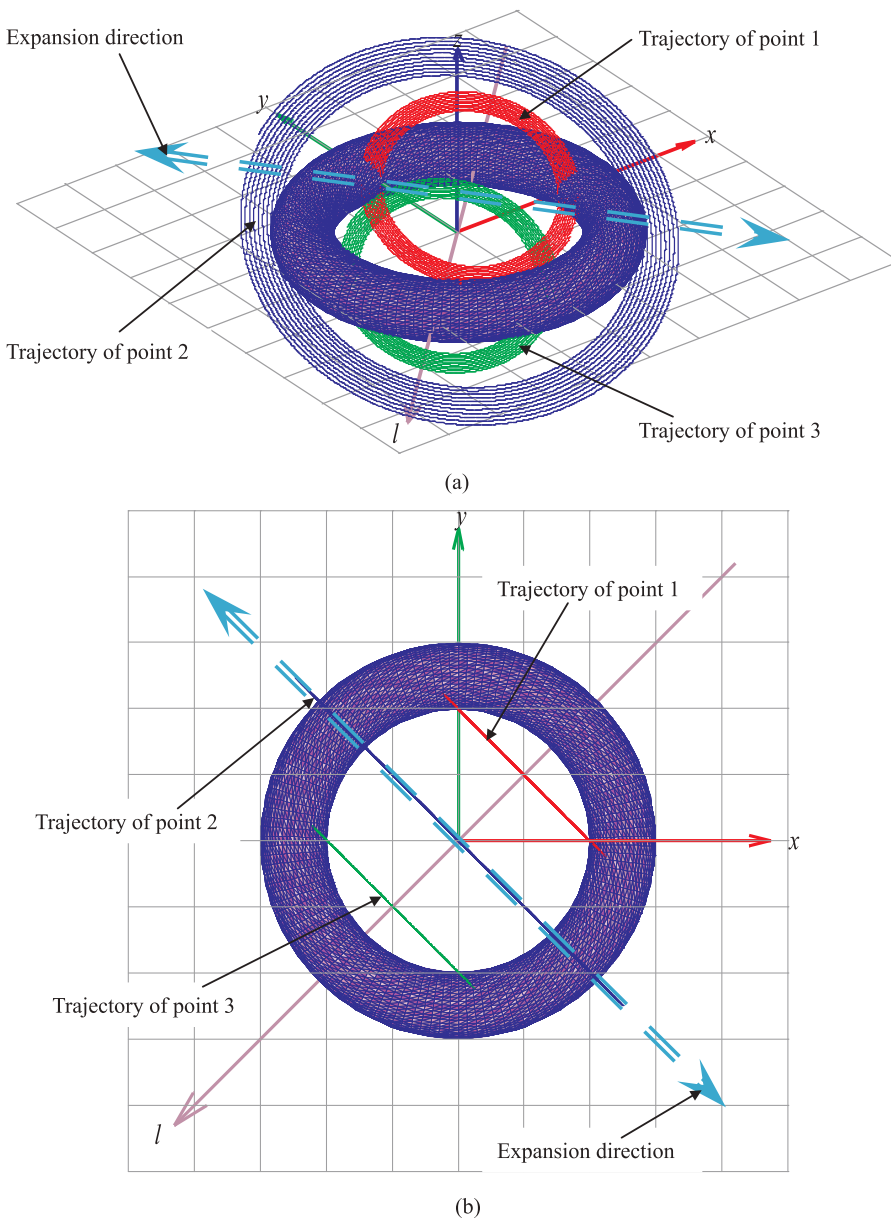


Fig. 15. Torus and the trajectories of CPs: (a) 3D view predicted by DDA⁰, (b) 2D view predicted by DDA⁰, (c) 3D view predicted by DDA¹, (d) 2D view predicted by DDA¹; (e) 3D view predicted by DDA* and (f) 2D view predicted by DDA*.

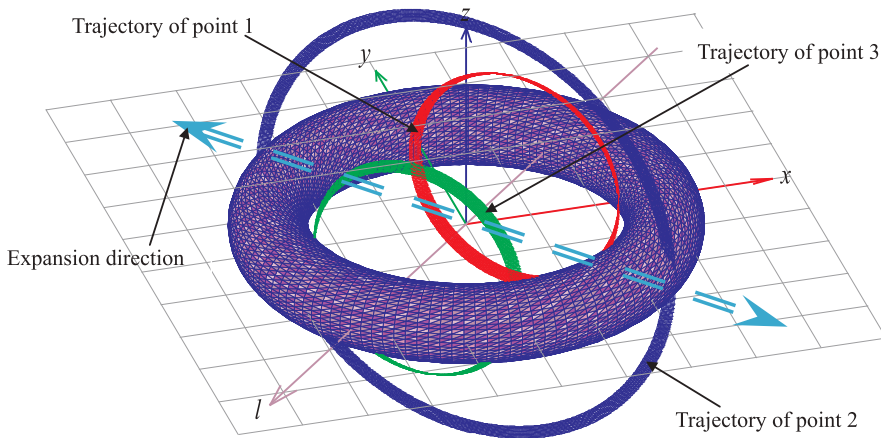
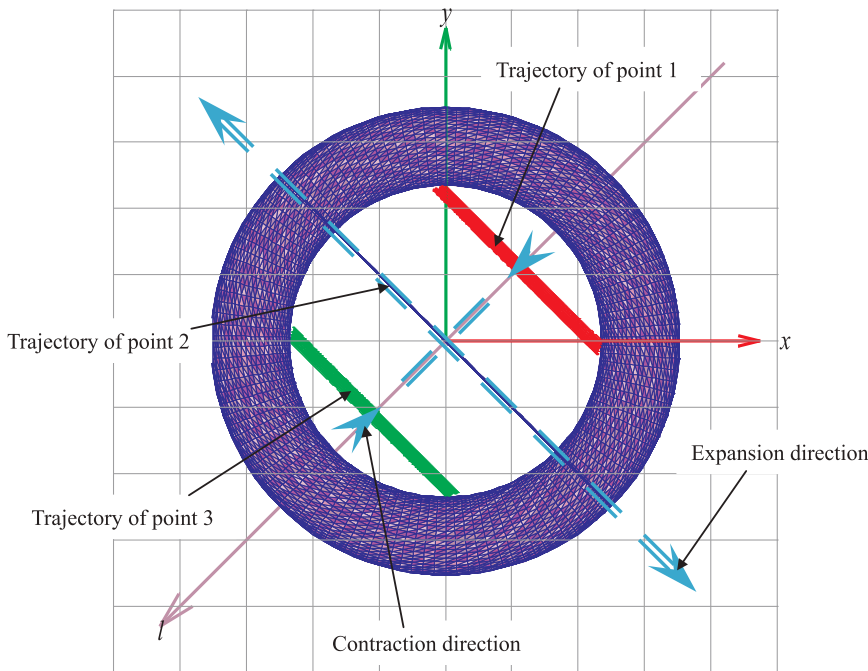


Fig. 15. (continued)

(c)



(d)

spectral radius of the generalized- α method [41] is given by $\rho_\infty = 1$.

During the simulation, we will observe the change of lengths of line segments OA and OB, which are perpendicular intersections and the line segment OB is coincident with the rotation axis, as well as sections O_1, O_2, O_3 and O_4 . For the initial time $CS = 0$, the lengths of OA and OB are all set equal to 5.0000 m; Sections O_1, O_2, O_3 and O_4 are all the circles with two dimensions of 2.0000 m and 2.0000 m, respectively, as shown in Fig. 12.

When $CS = 1000$, the results obtained by DDA^0, DDA^1 and DDA^* are shown in Fig. 13.

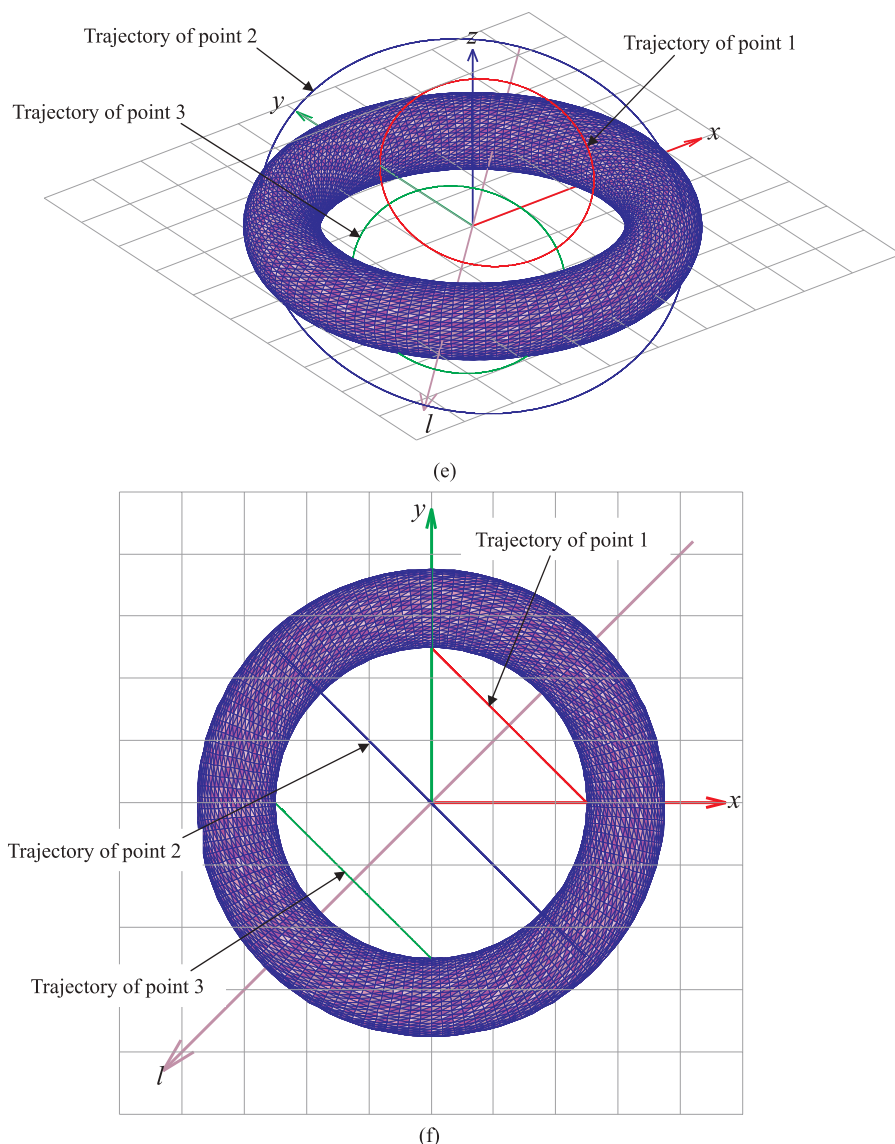
As shown from Fig. 13(a), the lengths of line segments OA and OB are 5.0000 m and 5.1266 m, respectively, and both sections O_1 and O_2 have a two-dimensional size of 2.0000 m and 2.0506 m, which makes sections O_1 and O_2 become to two ellipses. For Sections O_3 and O_4 , the two dimensions are equal to the 2.0506 m, which renders them remain to be circles. This indicates, for DDA^0 , equal expansions in the two directions perpendicular to the axis of rotation occur, while there is no change in the direction parallel to the axis of rotation.

As for DDA^1 (see Fig. 13(b)), It can be found that the lengths of line segments OA and OB are 4.9379 m and 5.0648 m, respectively. Moreover, for sections O_1 and O_3 , the dimensions parallel to the axis of rotation are both equal to 1.9752 m; while in the direction perpendicular to the axis of rotation the dimensions are 2.0117 m. Sections O_1 and O_3 become thus two ellipses. For sections O_2 and O_4 , the two dimensions are 2.0134 m and 2.0116 m, respectively. Hence, sections O_2 and O_4 are no longer circles. Regarding sections O_1, O_2, O_3 and O_4 , the two dimensions in the direction perpendicular to the axis of rotation are 2.0116 m and 2.0117 m, very close to each other.

Fig. 13(b) implies that, for DDA^1 , there are non-equal expansions in the two directions perpendicular to the axis of rotation and contractions in the direction parallel to the axis of rotation.

As for the case of DDA^* , it can be observed from Fig. 13(c) that the lengths of line segments OA and OB are 4.9999 m and 5.0000 m, respectively; Moreover, sections O_1, O_2, O_3 and O_4 have the two dimensions of 2.0001 m and 2.0000 m, respectively. This implies that there are no expansions or contractions in either direction perpendicular to or

Fig. 15. (continued)



parallel to the axis of rotation.

Fig. 14 further show results when the calculation is continued up to CS = 8000.

Based on DDA⁰, the simulation predicts that the length of line segment OA remains 5.0000 m with the simulating time, while that of line segment OB is elongated to 6.3350 m at CS = 8000, as shown in Fig. 14(a). As for sections O₁ and O₃, the two related dimensions are 2.0000 m and 2.5340 m, respectively, and those corresponding to Section O₂ and O₄ are enlarged to 2.5340 m. Evidently, there is no change in the dimension parallel to the axis of rotation, while there is continuing expansion in direction perpendicular to the axis of rotation. As a result, the ellipses O₁ and O₃ become more flat and the circles O₂ and O₄ expand larger.

From Fig. 14(b), the predictions by DDA¹ show that the lengths of line segments OA and OB are 4.4152 m and 5.3224 m, respectively. Sections O₁ and O₃ have the same two dimensions, namely 1.7650 m and 2.1290 m, whereas the two dimensions of sections O₂ and O₄ are 2.1289 m and 2.1290 m, respectively, which remains an ellipse even though they are very close to circles. Referring to Fig. 14(b), one can safely conclude that the predictions by DDA¹ show noticeable non-physical expansions and contractions.

While for DDA* as shown in Fig. 14(c), the length of line segment OA remains 5.0000 m as its original value. Moreover, the length of line segment OB appears to be expanded slightly from its original value 5.0000 m to 5.0016 m. This expansion is only 0.032% which can be negligible. For the same reason, the related dimensions of sections O₁, O₂, O₃ and O₄ obtained by DDA* can be considered not changed, as shown in Fig. 14(c). Therefore, we conclude that the expansions and contractions predicted by DDA* are vanishingly small and can be totally neglected.

In addition, the torus at CS = 8000 and the trajectories of three checking points from CS = 0 to CS = 8000 are shown in Fig. 15 corresponding to DDA⁰, DDA¹ and DDA*.

Due to the expansion along the direction perpendicular to the axis of rotation, there is an offset outward for each of the trajectories of points 1, 2 and 3, and each trajectory becomes a coplanar circular ring, as shown in Fig. 15(a). Moreover, these trajectories show like the three line segments in Fig. 15(b), indicating no occurrence of nonphysical expansion or contraction in the direction parallel to the axis of rotation, which is consistent with the conclusions drawn from Figs. 13(a) and 14(a).

For DDA¹, because the two phenomena of expansion and

Table 3
Volume of a torus corresponding to dual-axial rotation.

Time (CS)	DDA ⁰		DDA ¹		DDA [*]	
	CV (m ³)	ER (%)	CV (m ³)	ER (%)	CV (m ³)	ER (%)
100	98.9086	0.5012	98.4153	0.0000	98.4152	-0.0001
200	99.4043	1.0049	98.4153	0.0000	98.4153	0.0000
500	100.9066	2.5314	98.4153	0.0000	98.4153	0.0000
1000	103.4610	5.1269	98.4153	0.0000	98.4153	0.0000
2000	108.7654	10.5168	98.4152	-0.0001	98.4153	0.0000
5000	126.3669	28.4017	98.4152	-0.0001	98.4153	0.0000
8000	145.0600	47.3958	98.4151	-0.0002	98.4153	0.0000

Analytical solution: Volume = 98.4153 m³.

(CS: calculation step, CV: calculation value, RE: relative error).

contraction exist at the same time, the three trajectories are all offset outward. But due to point 2 is in the symmetry plane, its trajectory is a coplanar circular ring; while the trajectory of points 1 or 2 is not coplanar but contracts along the direction parallel to the axis of rotation and expands along the direction perpendicular to the axis of rotation, as shown in Fig. 15(c) and (d).

For DDA^{*}, because neither expansions nor contractions are found, each of trajectories of points 1, 2 and 3 remains a perfect circle in the 3D view and appears like a line segment in the 2D view, as shown in Fig. 15(e) and (f). In other words, from CS = 0 to CS = 8000, the torus has almost no deformation; which is in contrast with the predictions by DDA⁰ and DDA¹.

Some relative detailed data are further summarized in Table 3, which shows that the volume given by DDA⁰ is continually increased and the volume obtained by DDA¹ almost keeps at a constant value at the cost of contraction in the direction parallel to the axis of rotation, and the predictions by DDA^{*} remain the same.

5. Conclusions

We presented a 3D dynamic deformation formulation based on the S-R decomposition theorem that can simultaneously and accurately describe the strain and local rotation of deformable body. Similar to its counterpart in 2D, the new 3D dynamic formulation may capture the strains and local rotations and is generic and independent of numerical methods to be used. Therefore, it can be easily implemented in such popular methods as FEM, GFEM/XFEM and NMM. We showcased the 3D dynamic formulation by applying it to DDA and developed an S-R-decomposition-based DDA method, namely SR-3D-DDA. The robustness and effectiveness of the new formulation were demonstrated by several interesting examples, where the new method does not yield nonphysical expansions or contraction. Next, we will focus on three-dimensional contact detection and treatment.

Acknowledgements

This study is partially supported by the University Grants Council of Hong Kong through a Collaborative Research Fund (CRF) Project C6012-15G. This study is also supported by the National Basic Research Program of China (973 Program, Grant No. 2014CB047100); and the National Natural Science Foundation of China (Grant Nos. 11172313 and 51538001).

References

[1] Argyris JH. Matrix analysis of three-dimensional elastic media-small and large displacements. *AIAA J* 1965;3(1):45–51.
 [2] Argyris JH. Three-dimensional anisotropic and inhomogeneous elastic media matrix analysis for small and large displacements. *Arch Appl Mech* 1965;34(1):33–55.
 [3] Sukumar N, Moës N, Moran B, Belytschko T. Extended finite element method for three-dimensional crack modelling. *Int J Numer Methods Eng*

2000;48(11):1549–70.
 [4] Moës N, Gravouil A, Belytschko T. Non-planar 3D crack growth by the extended finite element and level sets—Part I: mechanical model. *Int J Numer Methods Eng* 2002;53(11):2549–68.
 [5] Gravouil A, Moës N, Belytschko T. Non-planar 3D crack growth by the extended finite element and level sets—Part II: level set update. *Int J Numer Methods Eng* 2002;53(11):2569–86.
 [6] Areias P, Belytschko T. Analysis of three-dimensional crack initiation and propagation using the extended finite element method. *Int J Numer Methods Eng* 2005;63(5):760–88.
 [7] Duarte CA, Babuka I, Oden JT. Generalized finite element methods for three-dimensional structural mechanics problems. *Comput Struct* 2002;77(2):215–32.
 [8] Duarte CA, Hamzeh ON, Liszka TJ, Tworzydło WW. A generalized finite element method for the simulation of three-dimensional dynamic crack propagation. *Comput Methods Appl Mech Eng* 2001;190(15):2227–62.
 [9] Johnson GR, Beissel SR, Stryk RA. A generalized particle algorithm for high velocity impact computations. *Comput Mech* 2000;25(2–3):245–56.
 [10] Johnson GR, Stryk RA. Conversion of 3D distorted elements into meshless particles during dynamic deformation. *Int J Impact Eng* 2003;28(9):947–66.
 [11] Rabczuk T, Belytschko T. Cracking particles: a simplified meshfree method for arbitrary evolving cracks. *Int J Numer Methods Eng* 2004;61(13):2316–43.
 [12] Rabczuk T, Belytschko T. A three-dimensional large deformation meshfree method for arbitrary evolving cracks. *Comput Methods Appl Mech Eng* 2007;196(29):2777–99.
 [13] Rabczuk T, Belytschko T. Adaptivity for structured meshfree particle methods in 2D and 3D. *Comput Methods Appl Mech Eng* 2005;63(11):1559–82.
 [14] Shi GH. Manifold method of material analysis. In: *Transactions of the 9th Army Conference on Applied Mathematics and Computing*. Report No. 92-1, US Army Research Office, Minneapolis, MN; 1991. p. 57–76.
 [15] Cheng YM, Zhang YH. Formulation of a three-dimensional numerical manifold method with tetrahedron and hexahedron elements. *Rock Mech Rock Eng* 2008;41(4):601–28.
 [16] He L, An XM, Ma GW, Zhao ZY. Development of three-dimensional numerical manifold method for jointed rock slope stability analysis. *Int J Rock Mech Min Sci* 2013;64:22–35.
 [17] He L, An XM, Zhao ZY. Development of contact algorithm for three-dimensional numerical manifold method. *Int J Numer Methods Eng* 2014;97(6):423–53.
 [18] Cundall PA. Formulation of a three-dimensional distinct element model—Part I A scheme to detect and represent contacts in a system composed of many polyhedral blocks. *Int J Rock Mech Min Sci Geomech Abstracts* 1988;25(3):107–16.
 [19] Hart R, Cundall PA, Lemos J. Formulation of a three-dimensional distinct element model—Part II Mechanical calculations for motion and interaction of a system composed of many polyhedral blocks. *Int J Rock Mech Min Sci Geomech Abstracts* 1988;25(3):117–25.
 [20] Belytschko T, Liu WK, Moran B, Elkhodary K. *Nonlinear Finite Elements for Continua and Structures*. John Wiley & Sons; 2013.
 [21] Fan H, Zheng H, He SM. S-R decomposition based numerical manifold method. *Comput Methods Appl Mech Eng* 2016;304:452–78.
 [22] Shi GH. Discontinuous deformation analysis: a new numerical model for the statics and dynamics of block system. PhD thesis. Univ Calif Berkeley, Berkeley, California; 1988.
 [23] Shi GH. Three dimensional discontinuous deformation analyses. DC Rocks 2001, The 38th US Symposium on Rock Mechanics (USRMS). American Rock Mechanics Association; 2001.
 [24] Jiang QH, Yeung MR. A model of point-to-face contact for three-dimensional discontinuous deformation analysis. *Rock Mech Rock Eng* 2004;37:95–116.
 [25] Wu JH, Juang CH, Lin HM. Vertex-to-face contact searching algorithm for three-dimensional frictionless contact problems. *Int J Numer Methods Eng* 2005;63:876–97.
 [26] Beyabanaki SAR, Mikola RG, Hatami K. Three-dimensional deformation analysis (3-D DDA) using a new contact resolution algorithm. *Comput Geotech* 2008;35:346–56.
 [27] Liu J, Geng QD, Kong XJ. A fast common plane identification algorithm for 3D contact problems. *Comput Geotech* 2009;36:41–51.
 [28] Wu W, Zhu HH, Zhuang XY, Ma GW, Cai YC. A Multi-shell cover algorithm for contact detection in the three dimensional discontinuous deformation analysis. *Theor Appl Fract Mech* 2014;72:136–49.
 [29] Shi GH. Contact theory. *Sci China Tech Sci* 2015;58:1–47.
 [30] Zheng F, Jiao YY, Gardner M, Sitar N. A fast direct search algorithm for contact detection of convex polygonal or polyhedral particles. *Comput Geotech* 2017;87:76–85.
 [31] Beyabanaki SAR, Jafari A, Biabanaki SOR, Yeung MR. Nodal-based three-dimensional deformation analysis (3D-DDA). *Comput Geotech* 2009;36:359–72.
 [32] Beyabanaki SAR, Bagtzoglou AC. Three-dimensional discontinuous deformation analysis (3-D DDA) method for particulate media applications. *Geomech Geoenviron* 2012;7(4):239–53.
 [33] Jiao YY, Huang GH, Zhao ZY, Zheng F, Wang L. An improved three-dimensional spherical DDA model for simulating rock failure. *Sci China Tech Sci* 2015;58(9):1533–41.
 [34] Jiao YY, Zhao Qiang, Zheng F, Wang L. Latest advances in discontinuous deformation analysis method. *Sci China Tech Sci* 2017;60(6):963–64.
 [35] Ke TC. The issue of rigid body rotation in DDA. In: *Proceedings of the first international forum on discontinuous deformation analysis (DDA) and simulation of discontinuous media*, Berkeley; 1996. p. 318–25.
 [36] Wu JH, Ohnishi Y, Nishiyama S. A development of the discontinuous deformation analysis for rock fall analysis. *Int J Numer Anal Methods Geomech* 2005;29:971–88.

- [37] MacLaughlin MM, Sitar N. Rigid body rotation in DDA. In: Proceedings of the first international forum on discontinuous deformation analysis (DDA) and simulation of discontinuous media, Berkeley; 1996. p. 620–35.
- [38] Cheng YM, Zhang YH. Rigid body rotation and block internal discretization in DDA analysis. *Int J Numer Anal Methods Geomech* 2000;24(6):567–78.
- [39] Jiang W, Zheng H. An efficient remedy for the false volume expansion of DDA when simulating large rotation. *Comput Geotech* 2015;70:18–23.
- [40] Chen ZD. On the representation of finite rotation in nonlinear field theory of continuum mechanics. *Appl Math Mech* 1986;7(11):1017–26.
- [41] Chen ZD. *Rational Mechanics*. China, Xuzhou: China Univ Min Press; 1988. [in Chinese].
- [42] Qin Z, Chen ZD. Large deformation analysis of shells with finite element method based on the S-R decomposition theorem. *Comput Struct* 1988;30(4):957–61.
- [43] Shang Y, Chen ZD. On the objective stress rate in co-moving coordinate system. *Appl Math Mech* 1989;10(2):103–12.
- [44] Li P, Chen ZD. The updated co-moving coordinate formulation of continuum mechanics based on the S-R decomposition theorem. *Comput Methods Appl Mech Eng* 1994;114:21–34.
- [45] Crisfield MA. *Non-linear finite element analysis of solids and structures—Volume 2: advanced topics*. Chichester: John Wiley & Sons; 1997.
- [46] Hamilton WR. *Elements of quaternions*. Cambridge: Cambridge University Press; 1899.
- [47] Spring KW. Euler parameters and the use of quaternion algebra in the manipulation of finite rotations: a review. *Mech Mach Theory* 1986;21(5):365–73.
- [48] Wehage RA. *Quaternions and Euler parameters—a brief exposition. Computer aided analysis and optimization of mechanical system dynamics*. Springer, Berlin, Heidelberg; 1984. p. 147–80.
- [49] <http://www.continuummechanics.org/rotationmatrix.html>.
- [50] Chung J, Hulbert GM. A time integration algorithm for structural dynamics with improved numerical dissipation: the generalized- α method. *J Appl Mech* 1993;60(2):371–5.
- [51] Fan H, He SM. An angle-based method dealing with vertex-vertex contact in the two-dimensional discontinuous deformation analysis (DDA). *Rock Mech Rock Eng* 2015;48:2031–43.
- [52] Newmark NN. A method of computation for structural dynamics. *J Eng Mech Div Proc ASCE* 1959;85(EM3):67–94.